An Ultra-Low-Cost Semi-Rigid Cable-Driven Knee Exoskeleton for Equitable Orthopedic Rehabilitation

Anthony Wu

Milton Academy

Abstract

This paper proposes the design, fabrication, and experimental validation of an ultra-low-cost semi-rigid cable-driven knee exoskeleton to address critical inequities in orthopedic rehabilitation access across low- and middle-income countries (LMICs). Anterior cruciate ligament ruptures, meniscal tears, and degenerative knee osteoarthritis account for over 50% of global knee disorders, imposing severe lower-limb disability on an estimated 500 million patients worldwide. With LMIC per-capita health expenditure falling below USD 200 per annum, commercially available exoskeletons priced at USD 80,000–100,000 remain entirely inaccessible. The proposed system achieves a bill of materials not exceeding USD 200, establishing a fiscally viable alternative for resource-limited settings. The device integrates a self-adaptive semi-rigid chain structure with a distributed load-anchoring system, reconciling the rigidity limitations of traditional rigid exoskeletons with the actuation deficiencies of soft exosuits. An ESP32-based embedded control architecture enables closed-loop torque regulation across three configurable rehabilitation modes, spanning 0° to 145° range of motion. The system delivers a minimum assistive torque of 10 Nm, weighs under 2 kg, and supports donning within 30 seconds, with field repairability via 3D-printed components. Prototype validation on a life-size anthropomorphic mannequin demonstrated high repeatability with inter-trial leg angle deviation of ≤1°. Joint alignment analysis further demonstrated a mean misalignment of 1.39 mm and an RMS misalignment of 2.55 mm across the full range of motion, indicating accurate tracking of the knee's instantaneous center of rotation. An on-device intelligent analytics framework integrates K-Means clustering, statistical trend analysis, and large language model (LLM)-generated recommendations, enabling personalized rehabilitation guidance without cloud dependency. Clinical relevance was supported through physiotherapist evaluation, achieving 94% agreement between AI-generated recommendations and expert rehabilitation protocols. This work establishes a replicable, clinically viable design paradigm for mitigating global rehabilitation inequity.

Keywords: knee exoskeleton; cable-driven actuator; orthopedic rehabilitation; semi-rigid exoskeleton; K-Means clustering; large language model; inertial measurement unit; closed-loop torque control; wearable robotics; range of motion; musculoskeletal disorders

1. Introduction

1.1 Research Background and Significance

Anterior cruciate ligament (ACL) ruptures, meniscal tears, and degenerative knee osteoarthritis (OA) collectively account for over half of all lower-limb disability-adjusted life years (DALYs) globally, imposing substantial burdens on motor function, occupational capacity, and health-related quality of life. Although reconstructive surgery and evidence-based physiotherapy can restore near-normal knee function, access to these interventions remains severely constrained by socioeconomic stratification and geographic disparity.

Even within high-income countries, structural inequities carry measurable clinical consequences. A landmark multi-center U.S. study demonstrated that patients in the highest-poverty quintile waited approximately 30% longer for ACL reconstruction, with each month of surgical delay associated with a 5% incremental reinjury risk — compounding secondary pathology including meniscal damage and accelerated cartilage degeneration. Globally, disparities are considerably more severe: approximately 47% of rural older adults in India present with symptomatic knee OA, yet fewer than 30% receive organised rehabilitation. In Chile, publicly insured patients are 2.2 times less likely to undergo knee replacement surgery than privately insured counterparts, illustrating the broader pattern whereby rehabilitation access is governed by economic circumstance rather than clinical need.

For an estimated 5 billion individuals lacking timely surgical access, conservative management remains the only viable option. Standard elastic braces provide minimal biomechanical support, while rigid post-operative orthoses impair proprioception, risk pressure injuries, and in many low- and middle-income country (LMIC) contexts, cost in excess of one month's median household income. At the technological frontier, commercial robotic exoskeletons such as ReWalk and Ekso are priced between USD 80,000 and USD 100,000, and even comparatively affordable platforms such as Roam Robotics Ascend retail at approximately USD 7,000 — entirely incompatible with LMIC per-capita health expenditure, which frequently falls below USD 200 per annum. This inaccessibility systematically excludes the highest-need populations from robotic rehabilitation, perpetuating cycles of disability, unemployment, and socioeconomic marginalisation.

The development of an ultra-low-cost, high-performance knee rehabilitation exoskeleton for low-resource settings is therefore both clinically urgent and ethically compelling. Such a device would bridge the gap between passive bracing and prohibitively expensive robotic platforms, democratise rehabilitation access, and contribute meaningfully to reducing the global orthopaedic disease burden. This study is motivated by precisely this translational imperative.

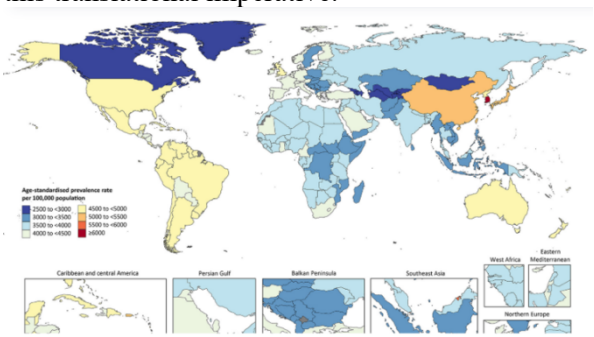

Figure 1-1: Global distribution of knee osteoarthritis prevalence and per capita health expenditure in low- and middle-income countries (to be supplemented)

1.2.1 Existing Knee Rehabilitation Devices and Exoskeletons

A variety of knee rehabilitation devices – from large clinical robots to wearable exoskeletons – have been developed, each with different approaches (rigid, soft, or hybrid designs) and corresponding trade-offs. Rigid exoskeletons (often used in hospitals and rehab centers) typically have metal frames with electric or hydraulic actuators at the joints. They provide strong assistance and precise joint angle control. For example, Zeilig et al (2012) found that the ReWalk and Ekso GT exoskeletons use powered knee and hip joints to enable gait training for people with paralysis. These rigid devices can supply substantial torques to support body weight or mobilize an immobile limb. However, they tend to be bulky and extremely costly. A full lower-limb exoskeleton like ReWalk weighs around 20 kg (with batteries and motors)\ and can

cost on the order of $70,000, putting it out of reach for most individuals outside institutional settings. The rigid metal frames also require careful alignment with the user's joints. If the exoskeleton's knee axis is even slightly misaligned, it can create shear forces and pain at the knee or skin interface .

Figure 1-2: ReWalk Exoskeleton

In fact, Bessler et al (2022) concluded that many early exoskeletons assumed a simple hinge knee and ignored the knee's translational motion, leading to user discomfort and "constraint" forces as the device fought the natural joint motion. Some advanced rigid designs address this by adding complexity. In a thorough investigation by Zhang et al(2021), it was found that many exoskeletons such as "It-Knee" and "AssiStep" include linkages or multi-axis joints to accommodate the shifting knee center, and the Samsung GEMS knee exoskeleton uses a cam-slider mechanism to track the knee throughout flexion While these solutions improve kinematic compatibility, they make the device heavier and more mechanically complex. In general, rigid exoskeletons offer reliable, reproducible motion guidance and high support torque, but at the expense of ergonomics – they are often heavy, expensive, and can be uncomfortable due to hard structure and alignment sensitivities.

Soft exoskeletons (exosuits) have emerged as a low-cost, lightweight alternative. These devices use flexible fabrics, straps, and Bowden cables or inflatable actuators instead of rigid frames. For instance, Sridar et al (2018) at Harvard developed soft exosuit shorts that assist hip extension and a soft knee exosuit prototype using pneumatic inflatable braces for post-stroke gait training. Soft exoskeletons are appreciated for their comfort and portability. The absence of rigid bars means they can conform to the body and usually weigh only a few kilograms at most. They inherently avoid joint misalignment issues because they don't impose a fixed hinge; the assistive forces are transmitted via cables or air muscles in parallel to the user's leg.

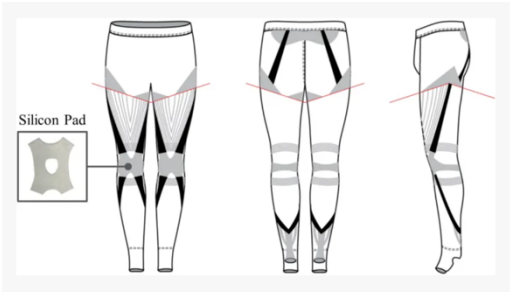

Figure 1-3: A Fully Soft and Passive Assistive Device to Lower the Metabolic Cost of Sit-to-Stand by Lee et. Al (2020)

This compliance can greatly improve wearer comfort and safety. However, soft systems come with their own challenges. Without a rigid frame, achieving high assistive torque is difficult – the textile can stretch and some force "leaks" through unwanted motion, generating less biomechanical assistance. Lee et al (2020) showed in a study of fully soft and positive assistive devices that across 6 testing trials, simulations of the exosuit estimated a maximum assisted knee torque of 0.03 Nm/kg, corresponding to about only 8.4% reduction in peak positive knee joint power (Figure 1-4). Control of soft exosuits is often less precise; force application can vary as the fabric shifts, and the effective moment arm at the joint may change during movement. Another shortcoming is that soft exos require very secure attachment (tight straps) to transmit force, which can cause pressure points or chafing on the user's limbs. Lee mentioned in the study that routing elastic bands produced concentrated pressure on the patella and misalignment of the kneecap. In summary, soft exoskeletons excel in lightness, adaptability, and cost, but generally provide lower support levels and can suffer from fit/anchoring issues (e.g. straps slipping or squeezing uncomfortably).

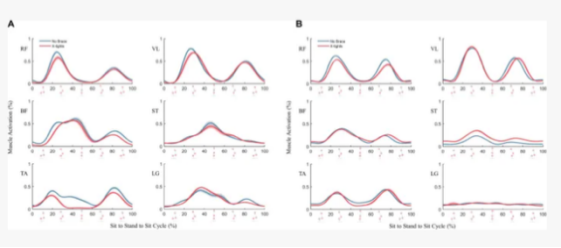

Figure 1-4: Caption Normalized EMG linear envelope for the STS cycle for (A) a participant who showed reduction in muscle activity and (B) a participant who showed similar activation patterns.

Semi-rigid or hybrid exoskeletons attempt to combine the best of both worlds. These designs include rigid elements where necessary for force transmission, but also incorporate flexible sections or compliance to maintain comfort and alignment. A notable example is the “Exo-Muscle” knee device developed by ZHang et al (2025) at the Istituto Italiano DI Tecnologia which uses a semi-rigid chain mechanism around the knee that this paper will adapt. In this design, a segmented linkage (which is flexible when unpowered) wraps around the joint and locks into a rigid shape when assisting, effectively creating a temporary external joint that moves with the knee This eliminates misalignment between the device and knee because the chain of segments conforms to the knee throughout its range, while providing a defined path for a tendon or cable that actuates the joint. Semi-rigid exoskeletons often use redundant degrees of freedom or compliant joints that allow slight translations or rotations, preventing the device from imposing incorrect forces on the limb. For example, Wang et al (2015) designed a semi-rigid exosuit based on an origami - inspired pneumatic actuator, The trade-off is that these semi-rigid suits are somewhat more complex than pure soft suits, requiring multi-layer training model such as the Koopman model by wang; Semi-rigid exoskeletons on the other hand, are far lighter and more ergonomic than fully rigid frames. Furthermore, Etenzi et al (2020) have reported that while rigid systems deliver more “deterministic” assistance (exact, controllable torques), solving misalignment via added joints made those systems heavier and less wearable, whereas soft systems solved misalignment but made consistent force output harder. For instance, a Chinese research team at CAS developed a “rigid–flexible coupled” knee-ankle exoskeleton that uses Bowden cable actuation and compliant joints to improve wearability while still providing needed torque (Cao et al, 2024). In general, current trends favor designs that maximize human–machine compatibility: minimizing device weight, improving alignment, and allowing natural joint movements.

1.2.2 Artificial Intelligence in Rehabilitation

Artificial intelligence (AI) is increasingly being integrated into rehabilitation medicine, offering clinicians novel tools to analyze complex patient data and support clinical decision-making. Lanotte, O'Brien, and Jayaraman (2023) provide a comprehensive overview of the current state of AI in rehabilitation, detailing both its promising applications across diverse data modalities and the substantial barriers that continue to impede its translation into everyday clinical practice.

At present, AI applications in rehabilitation draw upon several categories of healthcare data. Electronic health records (EHRs) constitute perhaps the most widely utilized data source, enabling AI models to perform automated screening, early disease detection, and prognostication. Models trained on routine EHR data have demonstrated the capacity to detect autism spectrum disorder in infants as early as 30 days after birth, identify individuals at elevated fall risk, and predict the development of pressure ulcers within the first 24 hours of intensive care unit admission. In stroke rehabilitation specifically, EHR-driven prognostic algorithms such as TWIST and PREP2 have shown promise in predicting walking recovery and upper limb function weeks to months following injury, providing clinicians with actionable information for care planning and goal setting.

Wearable sensor technology represents another significant avenue for current AI deployment in rehabilitation. Inertial measurement units, electromyography sensors, and consumer-grade smartwatches now enable continuous, high-resolution monitoring of patient movement and physiological parameters both within clinical settings and in the community. AI analysis of these signals has been applied to estimate dynamic balance in individuals with stroke, multiple sclerosis, and Parkinson's disease; assess motor deficits during standardized clinical tasks; detect tremor and bradykinesia; and monitor swallowing impairment in patients with dysphagia. Notably, research has demonstrated that integrating wearable sensor data into predictive models outperforms models relying solely on EHR and standard clinical information for outcomes such as post-stroke walking function. Beyond formal clinical assessments, AI applied to consumer wearables has been used to monitor postoperative recovery following pediatric surgery by identifying early signs of complications through patterns in activity, heart rate, and sleep data.

Video-based AI, leveraging advances in human pose estimation, is also being applied in present-day rehabilitation practice. These systems automatically detect body landmarks from standard camera footage to quantify gait, movement, and functional

impairment without the need for costly motion capture equipment. Current applications include gait analysis in individuals with Parkinson's disease and stroke, automated scoring of clinical assessments such as the Movement Disorder Society Unified Parkinson's Disease Rating Scale, and early prediction of cerebral palsy in infants through the General Movements Assessment. Instrumented environments, which use strategically placed sensors to monitor patients in a contactless manner, further extend AI's reach by enabling continuous vitals monitoring and symptom evaluation for conditions such as Parkinson's disease and COVID-19.

1.2.2 Shortcomings and Limitations of Current solutions

Despite many available devices, shortcomings remain that hamper wider adoption. A recent comprehensive review of physiotherapist and patient feedback by Morris et al (2023) identified several key issues with current lower-limb exoskeletons. Firstly, one-size-fits-all designs (poor personalization) created unnatural gait mechanics within patients. Stroke survivors in Vaughan - Graham et al. reported that rigid exoskeletons “felt unnatural” and made weight transfer harder. Difficulty donning and operating the device was also a challenge: in one stroke study, fitting the rigid exoskeleton took 30-40 minutes per session. Gautum et al. showed in graphical simulations of joint angles and stroke length that there is a nonlinear relationship between actuator stroke and knee angle. Figure 4 shows that since knee joint angle varies nonlinearly, it is difficult to achieve uniform torque or speed throughout sit to stand motion within rigid exoskeletos. Excessive weight (and poor weight distribution on the body) and high costs discussed earlier also limits the accessibility of such devices. The weight and placement of components are crucial – users report that carrying motors and batteries on the legs is tiring. High device cost is consistently cited as a barrier, limiting usage to wealthy hospitals or research labs. Even when cost is no object, discomfort and alignment issues can cause patients to reject the device. In the case of ReWalk, users must rely on crutches and perform exaggerated trunk leans to initiate steps, indicating that current devices for complete paraplegia still require significant user effort and adaptation. In summary, current knee rehab exoskeletons face a balance of effectiveness vs. practicality: rigid systems provide strong assistance but tend to be heavy, costly, and misaligned with natural anatomy, whereas soft systems are comfortable and light but provide limited support and can be hard to control precisely. These limitations point to the need for innovations that improve alignment, comfort, and cost-effectiveness.

Despite these diverse and demonstrably useful applications, there are major fundamental flaws with the usage of AI in rehabilitation. The first is a lack of interoperability. Patient data are frequently siloed across different care settings—primary care, acute hospitals, rehabilitation facilities, and community contexts—with limited standardization in how information is recorded and shared. This heterogeneity introduces bias and inaccuracy into AI models trained on such fragmented data, undermining their reliability and generalizability across institutions and patient populations.

The second major barrier is a lack of transparency. Most high-performing AI systems operate as "black boxes," providing outputs without interpretable explanations of their underlying computational logic. This opacity generates clinician distrust, particularly given that AI models are susceptible to errors and performance fluctuation during deployment. Without accessible and user-friendly frameworks for understanding how a model reached its conclusions, or what its potential sources of error are, widespread clinical adoption remains difficult. Efforts to address this through explainability techniques—such as feature importance analyses and symbolic metamodels—are ongoing but not yet standardized in rehabilitation contexts.

The third limitation concerns actionability. Even when AI generates accurate predictions or classifications, the insights produced are not always clinically meaningful or usable. For instance, an AI system identifying that a complex statistical feature derived from accelerometer data predicts injury risk may not translate into any concrete intervention a clinician can act upon. The disconnect between what is statistically predictive and what is clinically interpretable remains a persistent challenge, particularly when model-driving features do not reflect causal mechanisms but merely correlational associations within the training data.

Additional operational barriers compound these three primary limitations. These include constraints related to data storage, computational cost, patient privacy and security, regulatory compliance, and the limited

availability of large, diverse, and well-annotated training datasets. Rehabilitation populations are frequently small, heterogeneous, and clinically complex, making it difficult to compile datasets of sufficient size and representativeness to train generalizable models. Imbalanced datasets risk encoding biases related to race, gender, age, and socioeconomic status, potentially resulting in AI tools that perform inequitably across patient subgroups.

Given the breadth of comorbidities and functional impairments present in rehabilitation populations, training models capable of handling every clinical scenario is impractical. Until rigorous external validation and consistently low error rates are established, clinician oversight remains essential. Furthermore, deployed models require continuous monitoring and retraining to prevent data drift—the degradation of model performance that occurs when new patient data diverges from the characteristics of the original training set due to evolving clinical practices, disease patterns, or data acquisition methods.

A further infrastructural limitation, underexplored in the existing literature, is the heavy dependence of most published AI rehabilitation systems on cloud computing, high-bandwidth sensors, and costly hardware platforms. This reliance effectively excludes low-resource clinical environments and community settings from benefiting equitably from AI-driven rehabilitation tools, reinforcing existing disparities in access to advanced care. This gap foregrounds the relevance of embedded, hardware-efficient approaches to rehabilitation AI. The integration of lightweight machine learning algorithms—such as K-Means clustering and statistical trend analysis—with large language model API-based recommendation generation, deployed on low-cost microcontrollers such as the ESP32 and Arduino, represents a novel and practically significant contribution to the field. Such an architecture directly addresses the accessibility and scalability limitations identified throughout the literature, and situates low-power, on-device AI as a viable and necessary direction for the next generation of assistive and rehabilitative exoskeleton technologies.

2 Theoretical Design

The theoretical design of the semi-rigid cable-driven knee exoskeleton is grounded in the biomechanical characteristics of human knee motion and load transfer, drawing on the semi-rigid chain mechanism of the Exo-Muscle device . It focuses on solving key technical issues including tendon routing geometry optimization, moment arm stability, and torque-force requirement matching, while addressing the misalignment between traditional exoskeletons and the human knee joint, laying a solid theoretical foundation for the device's structural and hardware design.

2.1 Biomechanics of Human Knee Motion and Load Transfer

The human knee joint features complex kinematics with rolling and sliding motions during flexion-extension, resulting in a dynamically shifting instantaneous center of rotation (ICR) rather than a fixed hinge point.

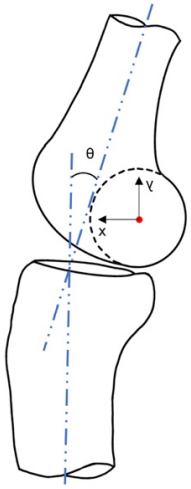

Figure 2.1 Knee Joint Diagram with J-Shaped instantaneous center of rotation path

In *Figure 2.1,* the femoral condyle articulates with the tibial plateau such that, at any given instant, the relative motion can be locally approximated as a pure rotation about an ICR (indicated by the red point, with associated x–y axes). The dashed circular arc represents this instantaneous rotational path, while the angle θ denotes the incremental angular displacement of the femur relative to the tibia. However, unlike an ideal revolute joint, the femoral condyle simultaneously rolls and translates (slides) along the tibial surface. This combined motion causes the location of the ICR to continuously migrate between successive instants of motion. As flexion progresses, the ICR traces a non-linear trajectory—commonly described as a "J-shaped" curve—shifting posteriorly and inferiorly due to the evolving contact geometry and ligament constraints. Consequently, accurate biomechanical modeling of the knee requires accounting for this moving ICR, as it fundamentally governs joint kinematics, moment arm variation, and force transmission during dynamic movement.

Traditional rigid exoskeletons with fixed hinge axes fail to adapt to this dynamic shift, leading to joint misalignment that generates undesired constraint and shear forces, causing user discomfort and even secondary injuries . Fully soft exoskeletons avoid misalignment via inherent flexibility but suffer from non-deterministic torque output due to unstable tendon routing, limiting their clinical efficacy .

A core design challenge for rehabilitation devices is balancing effective movement assistance and avoiding excessive joint loading—attaching heavy components distally on the limb increases inertial and gravitational loads on the knee . Thus, the design prioritizes lightweight composite and aluminum alloy materials, and positions actuators at the hip/waist to minimize distal limb weight, ensuring the device assists movement without imposing harmful additional loads on the recovering knee.

2.2 Tendon Routing Geometry and Moment Arm Mechanics

At the core of the design is a semi-rigid chain structure guiding the tendon around the knee. This mechanism switches between a flexible state (free knee motion) and a rigid state (taut tendon), combining the advantages of rigid and soft systems: it eliminates misalignment while ensuring a stable tendon routing path for deterministic torque output. The tendon routing path is designed via analytical geometry to meet two critical constraints:
(1) Clearance – a constant gap between the tendon and knee/limb at all flexion angles to avoid tissue contact and pressure;
(2) Stable moment arm – the perpendicular distance from the tendon to the knee's ICR remains in a

reasonable range, ensuring predictable assistive torque.

2.2.1 Coordinate System Definition and Routing Path Modeling

A coordinate frame is established at the knee joint center, with the y-axis along the shank and the x-axis in the sagittal plane. The tendon guiding route is a continuous piecewise function composed of elliptical and circular arcs, enabling smooth segment transition and adaptability to the knee's dynamic ICR:

$$f(x) = \begin{cases} \sqrt{b^2\left(1 - \frac{(x + x_c)^2}{a^2}\right)} - y_e & -0.034 \le x \le 0 \\ \sqrt{R^2 - (x + x_c)^2} - y_c & -0.171 \le x < -0.034 \end{cases}$$

where a, b are the ellipse semi-axes; R is the circle radius; x_c, y_c, x_e, y_e are offset parameters for continuous curve connection. All parameters are calibrated based on human lower limb biomechanical models to maintain clearance between the semi-rigid chain and knee tissues across the 0°–145° flexion range, and the device's adaptability to different body sizes is achieved via parameter and chain segment adjustments.

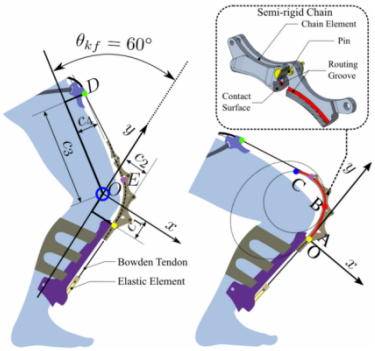

Figure 2.2 Tendon Routing Geometry model

Three key points define the routing path as seen in *Figure 2.2.* Point A (0, 0.015 m) as the chain start, Point B (-0.034 m, 0.128 m) as the ellipse-circle transition point, and Point C (-0.171 m, 0.139 m) as the chain end. This profile ensures the tendon crosses the knee without contact even at maximum flexion angles.

2.2.2 Tangency Condition and Moment Arm Calculation

Smooth force transmission requires tangential engagement between the tendon and the chain's routing groove, with the engagement point E (the tendon's first chain contact) satisfying the tangency condition :

$$f_k'(P_{E_x}) = \frac{f_k(P_{E_x}) - P_{D_y}}{P_{E_x} - P_{D_x}}$$

where $f_k(x)$ is the routing path function in the knee coordinate frame, translated from $f(x)$ by offsets between chain start A and the knee ICR; $f_k'(P_{E_x})$ is the first derivative of $f_k(x)$ at P_{E_x}; $P_D = (P_{D_x}, P_{D_y})$ is the thigh Bowden tendon anchor position, which varies with knee flexion angle θ_{kf} :

$$P_D = \begin{pmatrix} \cos\theta_{kf} & -\sin\theta_{kf} \\ \sin\theta_{kf} & \cos\theta_{kf} \end{pmatrix} \begin{pmatrix} c_4 \\ c_3 \end{pmatrix}$$

(c_3, c_4 are the y/x distances between point D and the knee ICR at $\theta_{kf} = 0°$).
The effective moment arm l_a (perpendicular distance from the knee ICR to the tendon's line of action) is calculated as :

$$l_a = \frac{|\overrightarrow{DE} \times \overrightarrow{DO}|}{|\overrightarrow{DE}|}$$

where $\overrightarrow{DE}$ is the vector from D to E, and $\overrightarrow{DO}$ is the vector from D to the knee ICR (coordinate origin). MATLAB simulations show the moment arm slightly decreases at 0°–30° flexion and increases for $\theta_{kf} > 30°$, ensuring stable torque output across the full range of motion. For real-time control and to avoid computational latency, the moment arm is fitted to a fifth-order polynomial :

$$L_a(\theta_{kf}) = -2.271e^{-12} \cdot \theta_{kf}^5 + 1.096e^{-9} \cdot \theta_{kf}^4 - 2.462e^{-7} \cdot \theta_{kf}^3 + 2.87e^{-5} \cdot \theta_{kf}^2 - 1.012e^{-3} \cdot \theta_{kf} + 0.074$$

where $L_a(\theta_{kf})$ is the moment arm (m) at knee flexion angle θ_{kf} (°).

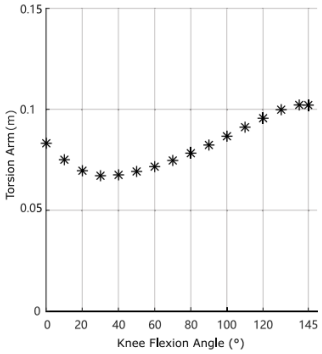

Figure 2-3: Moment arm variation with knee flexion angle (to be supplemented)

The actual knee assistive torque T_{exo} is the product of the measured tendon tension F_{tendon} and the effective moment arm l_a :

$$T_{exo} = F_{tendon} \cdot l_a$$

This relationship forms the basis for the control system to adjust motor output in real time.

2.2.3 Tendon Routing and Joint-Centered Kinematics

To express the tendon anchor's position relative to the lower leg during motion, a spatial transformation is applied to account for thigh segment rotation . Given a local exoskeleton anchor point p_t and flexion angle difference θ-φ, the global tendon contact position in the joint frame is computed as:

$$P = R_z(\theta - \varphi) \cdot p_t + P_t$$

where $R_z$is the 2D rotation matrix, and $P_t$is the thigh's global offset vector.This transformation enables the controller to continuously update the tendon direction and length as the thigh rotates relative to the shank. The torque generated by the cable is determined by the moment arm r (vector from the joint center to the contact point) :

$$r = P_O - P_C$$

where P_O is the torque reference point, and P_C is the calibrated rotation center.

2.2.4 Joint Angle Estimation and Inverse Kinematics

For inverse control or fallback knee angle estimation, the exoskeleton's geometry is used to map the actuator angle φ to the physiological flexion angle θ :

$$\theta(\varphi) = \cos^{-1}\left(\frac{X_{CO} - \ell_c \cos(\varphi - \alpha)}{r}\right) + \varphi$$

This analytical relationship verifies IMU readings and predicts tendon length requirements for the control system.

2.3 Torque and Force Requirements Analysis

The assistive torque requirement is derived from biomechanical data of quadriceps force during therapeutic knee extension: submaximal quadriceps force ranges from 150 N to 300 N, with a patellar tendon moment arm of 0.045–0.05 m , resulting in a knee extension torque range of 6.75–15 Nm. A design target of $\tau_{design} \geq 10$ Nm is set to meet the 95th-percentile rehabilitation demand and ensure motor longevity.

Adopting the Exo-Muscle's load analysis method , a simplified human joint-link mass model is used to verify the maximum tendon tension requirement, with the model incorporating thigh, shank, foot and upper body segments whose parameters are based on standard anthropometric data . Pinocchio dynamic computation library simulations are performed under various postures (ankle dorsiflexion: 0° to -40°; knee flexion: 0° to 145°; hip flexion: -15° to 125°) with a 20 kg hand payload, and the maximum required tendon tension is calculated as 323.9 N at the posture of ankle dorsiflexion -30°, knee flexion 50° and hip flexion 14° .

The DH03X brushed DC motor with a 20:1 spur gearbox is selected as the actuation component, providing a peak rated torque of 13.5 Nm and a 35% torque safety margin to compensate for frictional losses and transient dynamic loads :

$$\eta = \frac{\tau_{motor} - \tau_{design}}{\tau_{design}} = \frac{13.5 - 10}{10} = 0.35$$

Based on the torque-pulley radius relationship $\tau = F_{cable} \cdot r_{pulley}$, the required cable tension at the design torque is 400 N with a pulley radius of 0.025 m . The selected Dyneema cable has a minimum breaking load of ≥1200 N, yielding a tensile safety factor of 3, which exceeds the 323.9 N maximum required tension from dynamic simulations:

$$SF = \frac{F_{break}}{F_{cable}} = \frac{1200}{400} = 3$$

Considering the tendon routing's frictional efficiency reduction factor $\xi \approx 0.92$, the actuator needs to generate a compensated cable force of approximately 435 N, corresponding to a motor torque of 10.9 Nm. This value remains within the motor's peak specification and preserves a 24% post-friction torque margin , ensuring the device's stable operation under actual working conditions.

2.4 Series Elastic Element Selection and Modeling

To enhance user comfort and absorb impact loads, a series elastic element is integrated into the tendon transmission path, referencing the Exo-Muscle design . Tensile tests are conducted on two types of elastic elements (rubber belts and bungee cords), with selection criteria including the ability to reach the 323.9 N required tension within the recommended elongation range, compact integration with the calf attachment, and stable force-elongation characteristics .

Figure 2-3: Tensile test results of elastic elements

A 27.5 × 4.15 mm rubber belt is selected for its larger elongation range (0–200%), shorter initial length and simpler end fitting, which enables compact integration with the device . At maximum 200% elongation, the belt can provide a tension force exceeding 323.9 N, allowing the device to deliver up to 38 Nm of assistive torque at 145° knee flexion.The force-elongation relationship of the rubber belt is nonlinear, and thus fitted to a fifth-order polynomial for control system integration :

$$Y(F) = 2.803e^{-12} \cdot F^5 - 2.291e^{-9} \cdot F^4 + 5.882e^{-7} \cdot F^3 - 3.83e^{-5} \cdot F^2 + 3.674e^{-3} \cdot F$$

where $Y(F)$ is the elongation (m) at tension force F(N). This model is used to convert reference tension forces into actuator displacement commands in the control loop, ensuring precise force control.

2.5 Multibody Dynamic Modeling and Friction Compensation

A multibody dynamic model of the leg segment is established to compute the dynamic torque requirements of the knee during motion, considering inertial, gravitational and external loads :

$$m\left(\ddot{r} - r\dot{\theta}^2\right) = mg\sin\theta + f_r + f_e\cos(\varphi - \theta)$$
$$J\ddot{\theta} = \tau_r + \tau_a + \tau_f - \ell_c f\sin\gamma$$

where J is the moment of inertia of the leg segment; f_e is the external actuator force; ℓ_c is the leg segment length; τ_r, τ_a, τ_f are the restoring torque, actuator torque and frictional torque, respectively.

To address internal frictional losses in the cable path (especially through curved Bowden segments), a velocity-dependent friction model is incorporated :

$$f_{fr} = -k_u \cdot \mu_f \cdot \dot{u}$$

where μ_f is the friction coefficient; k_u is a system constant; $\dot{u}$ is the tendon velocity. The semi-rigid chain's guiding route is finely machined and lubricated to minimize friction, with transmission efficiency remaining above 85% within the 0°–100° cable deflection operational range , ensuring the tension force measured by the load cell closely approximates the actual tendon tension.

Additionally, a restoring torque model governs the response of the tendon's effective angle relative to a baseline configuration :

$$\tau_r = k_\theta(\theta_e - \theta_{e0})$$

where k_θ is the angular stiffness and θ_{e0} is the resting orientation. This behavior is reinforced by the series elastic element, enabling the device to achieve energy buffering and shock absorption, and further improving the human-machine interaction experience.

3 Structural Design

The structural design of the exoskeleton adheres to the principles of biomechanical alignment, lightweight, low cost and ergonomics, and is composed of three core parts: the semi-rigid chain structure, the distributed anchoring and load path structure, and the actuator/sensor mounting structure. The overall structure abandons the complex rigid frame of traditional exoskeletons, adopts a semi-rigid design to balance force transmission and motion flexibility, and realizes distributed load transfer to avoid concentrated pressure on the knee joint.

3.1 Overall Structural Design

The ultra-low-cost semi-rigid cable-driven knee exoskeleton is a modular structure, mainly consisting of the thigh segment, shank segment, semi-rigid chain guide mechanism, actuation module, sensor module, and distributed strap anchoring system (Figure 3-1). The thigh segments are constructed from lightweight aluminium alloy profiles, while the shank segments consist of a combination of lightweight aluminium alloy profiles and PETG 3D-printed components, ensuring structural rigidity while minimizing overall weight; the semi-rigid chain guide mechanism is connected between the thigh and shank segments, surrounding the lateral side of the knee joint to guide the Dyneema cable and avoid direct contact with the knee; the actuation module (DH03X motor + gearbox + cable spool) is mounted on the hip/waist via a backpack-style bracket to reduce distal limb weight and knee inertial load; the sensor module (dual MPU-6050 IMUs, HX711 load cell) is fixed on the thigh and shank rigid segments and in the cable transmission path, respectively; the distributed strap anchoring system includes waist belts, hip straps and thigh straps, which realize the fixed installation of the device and the distributed transfer of cable tension.

The overall structural design of the exoskeleton has the characteristics of simple assembly, easy wearing and adjustable size: quick-release mounts are set on the thigh and shank segments, enabling donning and doffing in under 30 seconds; a single Velcro/buckle strap at the mid-thigh serves as the main attachment point, reducing setup complexity; the length of the thigh/shank segments and the tightness of the straps are adjustable to adapt to users of different heights and body types; the electronics module is housed in a compact cavity on the backplate with a profile of ≤20 mm, ensuring the device's portability and wearability .

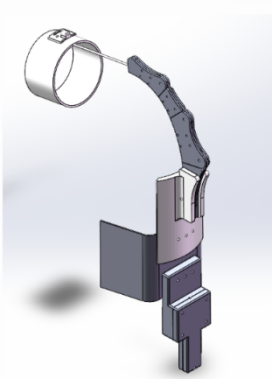

Figure 3-1: Overall structural design of the semi-rigid cable-driven knee exoskeleton

3.2 Semi-Rigid Chain Structure

The semi-rigid chain structure is the core mechanical component of the exoskeleton, responsible for guiding the tendon path and ensuring the consistency of the moment arm, and its design directly determines the device's assistive torque performance and biomechanical alignment . The chain consists of 12 interlocking polylactic acid (PLA) link segments connected by M3 stainless steel pivot pins (Figure 3-1), with each link having a 15° rotational freedom, providing a cumulative maximum deflection of 180° to adapt to the full range of knee flexion and extension (0°–140° for clinical rehabilitation).

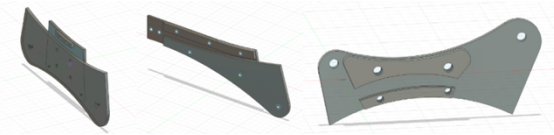

Fig 3-2: Singular components of 5 link chain

The semi-rigid chain maintains high lateral rigidity (transverse stiffness >50 N/mm) to prevent lateral deformation of the tendon path and ensure stable force transmission, while its longitudinal flexibility allows it to conform to the knee's dynamic motion trajectory, eliminating misalignment between the device and the knee joint. The links are shaped to match the lateral femur and tibia profiles of the human lower limb, distributing the contact pressure between the chain and the limb over a surface area of approximately 180 cm², with the contact pressure below the 20 kPa safe skin-contact pressure

threshold, avoiding pressure sores and discomfort caused by concentrated contact .

The PLA link segments are manufactured by 3D printing, which has the advantages of low cost, fast prototyping and easy customization, and the damaged links can be quickly replaced with 3D-printed spares, realizing the field repairability of the device – a key requirement for application in low-resource settings with limited maintenance resources. The M3 stainless steel pivot pins ensure the structural strength and durability of the chain, withstanding the repeated tensile and bending loads during rehabilitation exercise.

Fig 3-3: Integrated design onto a life size mannequin

3.3 Distributed Anchoring and Load Path Structure

To solve the problem of concentrated pressure on the knee joint caused by direct tendon anchoring in traditional soft exoskeletons, the design adopts a distributed anchoring and load path structure, which redirects the high tension of the Dyneema cable (up to ~324 N) to the waist, hip and thigh – the body parts with strong load-bearing capacity – avoiding direct pressure on the knee joint and the sensitive neurovascular structures around it (e.g., the common peroneal nerve) .

Inspired by the Exo-Muscle's strap routing design , the upper terminus of the Dyneema cable is anchored to a strap interface on the anterior side of the thigh, which splits into multiple straps: one main strap routes upwards to the waist belt, and two auxiliary straps wrap around the hip and posterior waist from the lateral side of the thigh. This load path design realizes the dynamic distribution of tension: during shallow knee bends (0°–60°), the anterior waist strap bears the main load; during deep bends (60°–140°), the posterior hip straps engage sequentially, shifting the load to the posterior waist and even providing auxiliary support for the hip joint, further reducing the load on the knee. The straps are made of high-elasticity, wear-resistant nylon fabric with breathable foam padding, which improves wearing comfort and prevents chafing of the skin.

The cable transmission path is designed with a Bowden cable conduit to protect the Dyneema cable, reduce frictional losses during cable movement, and ensure the stability of the tendon path. The cable spool driven by the motor is mounted on the hip/waist actuation module, and the cable is routed through the Bowden conduit to the semi-rigid chain on the lateral knee, then to the shank anchor point, forming a closed cable transmission loop that realizes the conversion of motor rotational motion into knee joint flexion/extension assistive force.

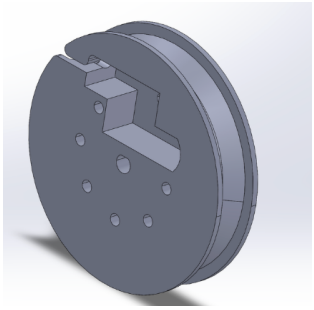

Figure 3.4 Bowden Conduit

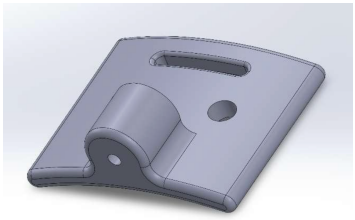

Figure 3.5 Thigh Anchor point and cable director

4 Hardware Design

The hardware design of the exoskeleton follows the principle of low cost, high reliability and easy integration, selecting commercial off-the-shelf low-cost electronic components and building a closed-loop control system consisting of a main control module, sensor module, actuation module, communication module and safety module. The total cost of core electronic components is less than US$150, which is the key to realizing the ultra-low cost of the whole device. The hardware system is integrated with the structural system, with reasonable layout and simple wiring, suitable for field use in low-resource settings.

4.1 Core Electronic Components

The core electronic components feature the ESP32 as the main control unit, paired with dual MPU-6050 IMUs, an HX711 load cell, a DH03X brushed DC motor with a 20:1 spur gearbox, a BT18 Bluetooth module, and an emergency-stop latch. These components complement each other in function, forming a complete hardware support system for the device, with the total cost of core electronic components below US$150.

(1) ESP32 Microcontroller: Serving as the main control unit, it is responsible for receiving and processing sensor data, executing control algorithms, and sending PWM drive signals to the motor. It features open-source design for easy development and rich peripheral interfaces, lowering the technical threshold for application in low-resource areas.

Figure 3-3: ESP32 Microcontroller

(2) Dual MPU-6050 IMUs: Mounted on the rigid thigh and shank segments respectively, they real-timely measure knee joint angle, angular velocity and gait phase information with high measurement accuracy and low power consumption. The differential measurement method improves the accuracy of gait recognition.

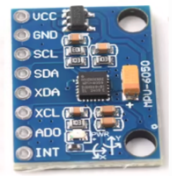

Figure 3-4: MPU 6050 sensors

(3) HX711 Load Cell: Connected in series in the transmission path of the Dyneema cable, it real-timely measures cable tension. Combined with the moment arm, it calculates the actual assistive torque, providing data support for torque adjustment and safety limit setting.

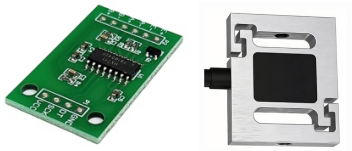

Figure 3-5: HX711 Load Cell and Tension sensor

(4) DH03X Brushed DC Motor with 20:1 Spur Gearbox: As the core actuation component, it amplifies motor torque to meet the device's assistive torque requirements, with high transmission efficiency and a compact structure, suitable for the lightweight design of the actuation module.

Figure 3-6: DH03X Brushed DC Motor

(5) BT18 Bluetooth Module & Emergency-Stop Latch: The BT18 Bluetooth module enables wireless communication between the device and mobile/web terminals, supporting remote control. The emergency-stop latch is a mechanical safety component that can slack the cable in emergency situations, ensuring the free movement of the user's limbs and improving the safety of device operation.

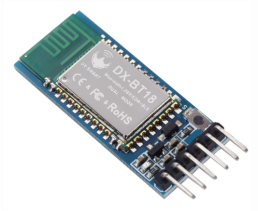

Figure 3-7: BT18

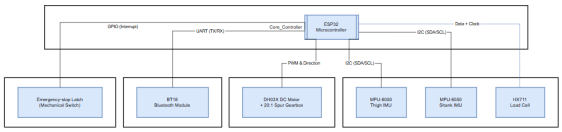

Figure 4-1: Schematic of the control circuit framework

4.3 Sensor and Actuator Integration

The sensor and actuator integration of the exoskeleton follows the principle of minimizing distal weight, ensuring sensing accuracy and stable force transmission, with a reasonable layout to realize the closed-loop control of "sensing-measurement-control-actuation" (Figure 4-2).

(1)**Sensor integration**: The two MPU-6050 IMUs are fixed on the inner side of the thigh and shank aluminium alloy segments via 3D-printed brackets, with the sensing axis aligned with the longitudinal axis of the limb to ensure the accuracy of angle measurement; the HX711 load cell is connected in the Dyneema cable path between the cable spool and the semi-rigid chain, with a fixed installation to avoid the influence of cable vibration on tension measurement; all sensors are connected to the ESP32 via shielded wires to reduce electromagnetic interference and ensure the stability of signal transmission.

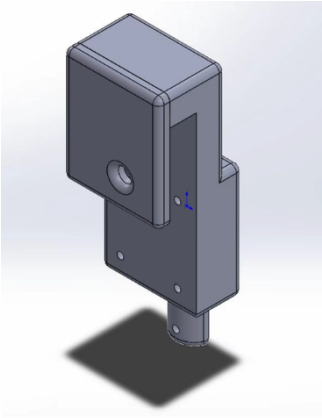

Figure 3- Load Cell Housing System

(2)**Actuator integration**: The DH03X motor + gearbox + cable spool actuation module is mounted on the hip/waist via a lightweight backpack-style bracket, far from the knee joint, which effectively reduces the distal weight of the limb and the inertial load on the knee during motion – a key design to avoid increasing the knee's joint force. The cable spool is aligned with the Bowden cable conduit inlet to ensure the smooth routing of the Dyneema cable and reduce frictional losses.

(3)**System integration**: All sensors and actuators are connected to the ESP32 main controller through standard communication and drive interfaces, forming a closed-loop sensing and actuation system. The sensor data is real-time transmitted to the main controller, which executes the control algorithm to generate the motor drive signal, and the actuator outputs the corresponding torque according to the signal, realizing the dynamic adjustment of the exoskeleton's assistive force based on the user's motion state. The distributed load path structure of the exoskeleton is combined with the actuator integration to ensure the stable transmission of the assistive force from the hip/waist to the knee joint via the Dyneema cable.

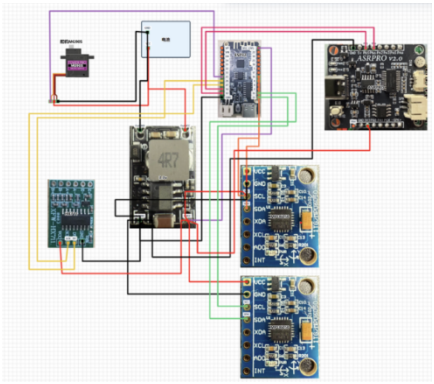

Figure 4-2: Schematic of sensor and actuator integration

4.4 Voice Interaction Submodule

To enhance the usability and autonomous operability of the device in low-resource settings, and to adapt to the needs of non-professional users (e.g., community patients, home rehabilitation populations), an offline voice interaction submodule is added. Guided by the design principles of low cost, offline operation, and low invasiveness, this submodule is seamlessly integrated with the ESP32 main controller without interfering with the existing closed-loop sensor control, actuator drive, or AI

analysis system logic. The incremental hardware cost is controlled within US$30, which is fully consistent with the core positioning of the device as "ultra-low cost".

(6) The core components of the voice interaction submodule include an LD3320 offline voice recognition chip (cost: US$15–20), an 8Ω/0.5W micro-speaker (cost: US$2–5), and an impedance matching circuit. It supports local command recognition and voice broadcasting without relying on a network, thus avoiding network limitations in low-resource scenarios. The submodule communicates with the ESP32 via a UART serial port (baud rate: 9600) with the following pin mapping: TX of the voice module → GPIO3 of the ESP32, RX of the voice module → GPIO2 of the ESP32, VCC connected to 3.3V, and GND for common grounding. Power is supplied by the ESP32 power domain, with a maximum operating current of ≤50mA, resulting in minimal impact on battery life. In terms of installation layout, the submodule is integrated into the electronic cavity (18×80×50mm) of the waist bracket, and an acoustic window is opened on the side of the speaker facing the user to ensure audio transmission efficiency while avoiding mechanical interference with the semi-rigid chain structure and sensor modules.

In terms of functional design, the submodule adopts a closed-loop logic of "wake-up-command-feedback": "Hey RENA" is set as the fixed wake-up word, and the submodule enters a 30-second command reception state after being awakened, automatically entering sleep mode after timeout to reduce power consumption. Core commands cover three major scenarios: mode switching, status query, and emergency control, with specific mappings as follows: "Start Free Training" triggers the Passive Support mode (feedback: "Free training started, please sit upright"), "Start Resistance Training" triggers the Graduated Resistance mode (feedback: "Resistance training started"), "Start High-Intensity Training" triggers the High-Intensity Strength mode (feedback: "High-intensity training started"), "Stop Training" stops all modes and unlocks the servo (feedback: "Training stopped"), "Current Progress" reads angle and force data (feedback: "Current angle X°, force YN"), and "Emergency Stop" triggers mechanical emergency unlocking (highest priority, feedback: "Emergency stop executed").

In terms of control priority design, the command priority from high to low is "Emergency Stop voice command > mechanical emergency switch > other voice commands > Bluetooth/Web commands" to ensure operational effectiveness in emergency scenarios. When multiple channel commands are triggered simultaneously, the ESP32 main controller prioritizes the execution of high-priority commands and notifies the user via voice feedback. The system integration process is shown in Figure 4-3, with the core link being "voice module (wake-up-recognition) → ESP32 controller (command parsing-priority judgment) → sensors/actuators (data collection/action execution) → voice module (feedback broadcasting)".

Test results show that the key performance indicators of the voice interaction submodule meet the requirements of rehabilitation scenarios: the recognition accuracy is ≥95% in quiet environments (≤40dB) and ≥90% in slightly noisy environments (50–60dB), and the total delay from command triggering to feedback completion is ≤500ms; when the device operates continuously with the voice function, the runtime remains ≥2.0 hours, which meets the design target without affecting the stability of the original hardware system.

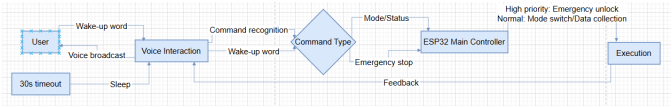

Figure 4-3 System Integration Flowchart of the Voice Interaction Submodule

5 AI Driven Analysis and Recommendation System

5.1 Software Architecture

The software intelligence model was designed as a modular, clinically oriented analytics platform capable to transform raw biomechanical data into interpretable rehabilitation insights in near real time. The system is implemented as a Python-based web application using a lightweight SQLite relational

database backend to ensure portability, low deployment cost, and compatibility with low-resource environments. This architectural decision aligns with the project's broader objective of accessibility, particularly in settings where complex cloud infrastructure or proprietary hospital systems are unavailable.

Incoming sensor data streams are transmitted at 2 Hz from the embedded controller via WiFi and received by the backend ingestion layer. Each packet contains timestamped force (N), joint angle (°), and auxiliary orientation data. Upon receipt, a data validation and quality scoring routine is executed to detect malformed packets, missing values, or out-of-range biomechanical readings. Validated data are written to the sensor_data table, which is relationally linked to training_sessions and users tables via foreign key constraints. This relational schema enforces data integrity while enabling longitudinal tracking of patient performance across sessions. The database structure was intentionally normalised to third normal form (3NF) to prevent redundancy and ensure analytical scalability.

Once a training session is marked as complete, the analysis engine executes five sequential computational stages:

1. **Statistical Characterisation** — computation of descriptive metrics over force and angle datasets.

2. **Trend Analysis** — temporal comparison within and across sessions to quantify rehabilitation progression.

3. **K-Means Performance Clustering** — unsupervised learning to identify performance states within the multidimensional feature space.

4. **Composite Performance Scoring** — transformation of multidimensional outputs into a clinically interpretable 0–100 index.

5. **LLM-Powered Recommendation Generation** — structured data serialization and submission to a large language model for personalized rehabilitation guidance.

Each analytical module is encapsulated as an independent Python class, allowing computational separation of concerns and facilitating unit-level validation. This modular design enables statistical methods, clustering algorithms, or scoring formulas to be iteratively refined without affecting upstream data ingestion or downstream recommendation logic.

The final stage integrates with the DeepSeek large language model API to generate structured rehabilitation recommendations. Analytical outputs are serialized into a deterministic JSON payload to preserve data fidelity before submission. The response is parsed and stored in the database, ensuring that all AI-generated recommendations remain audit-traceable and linked to the originating session data.

A mobile/web dashboard renders all analysis outputs through interactive visualizations, including force-time plots, range-of-motion trajectories, clustering maps, and performance score summaries. Therapists can review raw statistics alongside AI recommendations, preserving human oversight in the decision-making loop. The interface is deliberately designed to present both quantitative metrics and narrative interpretation, reducing cognitive load for clinicians while maintaining mathematical rigor.

The complete pipeline is illustrated in Figure 7. Raw sensor data undergo ingestion and validation before SQLite storage. Analytical modules operate in parallel branches, whose outputs converge within the performance scoring engine. The composite results are then transmitted to the DeepSeek API, and final recommendations are rendered within the dashboard interface. An inset entity-relationship diagram depicts the structured relationships between users, training_sessions, and sensor_data, highlighting referential integrity and longitudinal traceability.

This architecture balances computational robustness, interpretability, and deployability. By combining deterministic statistical modeling with probabilistic AI interpretation within a traceable database framework, the system ensures both analytical transparency and practical clinical usability—an essential requirement for translational biomedical engineering applications.

5.2 Statistical Analysis Module

The Statistical Analysis Module forms the quantitative foundation of the software analytics pipeline. Its primary objective is to convert raw time-series biomechanical signals into structured descriptive metrics that are clinically interpretable, mathematically rigorous, and reproducible. By summarizing force and joint angle data at the session level, this module provides the essential inputs for downstream trend modeling, clustering, and performance scoring.

For each completed training session, the system operates on a dataset

$$D = \{x_1, x_2, \dots, x_n\}$$

where x_i represents either a force measurement F_i in Newtons or an angle measurement θ_i in degrees recorded at 2 Hz. Data points are first sorted chronologically and validated to remove null or physiologically implausible values (e.g., negative force or angles beyond anatomical limits). Missing values are handled conservatively to preserve data integrity.

5.2.1 Descriptive Metrics

For each channel (force and angle), the following descriptive statistics are computed independently.

Mean (Central Tendency)

$$\mu = \frac{1}{n}\sum_{i=1}^{n} x_i$$

The mean provides an estimate of sustained output level across the session. For force, this reflects average muscular exertion; for angle, it represents average joint positioning.

Standard Deviation (Variability)

$$\sigma = \sqrt{\frac{1}{n-1}\sum_{i=1}^{n} (x_i - \mu)^2}$$

The standard deviation quantifies intra-session variability. In rehabilitation contexts, elevated force variability may indicate neuromuscular instability or fatigue, while excessive angular variability may reflect reduced motor control.

Median (Robust Central Estimate)

$$M_{n\ odd} = \frac{x_{(n+1)}}{2} \quad M_{n\ even} = \frac{x_{(n/2)} + x_{(n/2+1)}}{2}$$

The median is included to mitigate the influence of transient outliers such as sudden muscle spikes or brief sensor artifacts. In early rehabilitation stages, where motor control may be inconsistent, the median can provide a more representative central estimate than the mean.

Extrema (Physiological Bounds)

$$x_{min} = min(x_i), x_{max} = max(x_i),$$

For force data, Fmaxf_0F_{\max}Fmax represents peak muscular strength output during the session. For angle data, θminf_0\theta_{\min}θmin and θmaxf_0\theta_{\max}θmax define the achieved range of motion (ROM), a primary clinical indicator of joint recovery.

5.2.2 Descriptive Metrics

Statistics are computed independently for three training modalities. Force test uses the reported metrics $\mu_F, \sigma_{F,} F_{min}, F_{max}, M_F, n_F$. These metrics quantify muscular strength output and consistency. Angle tests uses the metrics $\mu_\theta, \sigma_{\theta,} F_\theta, F_\theta, M_\theta, n_\theta$. These quantify joint mobility and control. In a combined test, both force and angle metrics are computed simultaneously, enabling multi-dimensional biomechanical assessment.

5.2.4 Role Within the Analytical Pipeline

The Statistical Analysis Module provides deterministic numerical descriptors that feed directly into Trend differentials (Section 5.3), Cluster feature vectors (Section 5.4), Composite scoring normalization (Section 5.5), and structured LLM prompts (Section 5.6)

This system ensures transparency and reproducibility of every downstream calculation. This deterministic statistical core is critical for maintaining methodological credibility in a biomedical research context, particularly when integrating probabilistic AI recommendation systems.

In summary, the Statistical Analysis Module transforms high-frequency sensor streams into

clinically meaningful biomechanical summaries, establishing the quantitative baseline upon which all higher-level rehabilitation intelligence is constructed.

5.3 Role Within the Analytical Pipeline

The Trend Analysis Module was developed to quantify rehabilitation progression over time by transforming descriptive session statistics into longitudinal performance indicators. While per-session statistics characterize isolated training performance, meaningful rehabilitation assessment requires evaluation of directional change across repeated sessions. This module therefore introduces temporal comparison models that measure strength development, range-of-motion (ROM) recovery, and neuromuscular consistency across the rehabilitation timeline.

For each user, historical sessions

$$S = \{S_1, S_2, \ldots S_m\}$$

are retrieved from the relational database and sorted chronologically according to session timestamp. Within each session, sensor measurements form a time-ordered dataset

$$D = \{x_1, x_2, \ldots, x_n\}$$

Where x_i represents either force F_i or angle θ_i.The module evaluates both intra-session progression (fatigue or short-term adaptation) and inter-session progression (long-term rehabilitation improvement).

Intra-Session Midpoint Analysis

To detect within-session adaptation or fatigue patterns, each session dataset is partitioned at its midpoint:

$$D_{first} = D_{sorted}\left[1{:}\frac{n}{2}\right],$$

$$D_{second} = D_{sorted}\left[\frac{n}{2} + 1{:}n\right]$$

The mean force and angle are computed separately for each half. The change in force output across the session is defined as:

$$\Delta F = \mu(D_{second})_F - \mu(D_{first})_F$$

and the percentage change as:

$$\Delta F\% = \frac{\Delta F}{\mu(D_{first})_F} \cdot 100\%$$

Similarly, angular progression is calculated as:

$$\Delta\theta = \mu(D_{second})_\theta - \mu(D_{first})_\theta$$

$$\Delta\theta\% = \frac{\Delta\theta}{\mu(D_{first})_\theta} \cdot 100\%$$

A positive ΔF suggests progressive activation or warm-up strengthening, whereas a negative value may indicate muscular fatigue. For angle measurements, increasing mean values (in flexion-extension contexts) typically reflect improved dynamic ROM during the session. This midpoint methodology provides a computationally lightweight fatigue–adaptation estimator without requiring complex biomechanical modeling.

Inter-Session Longitudinal Comparison

To evaluate rehabilitation progress across multiple sessions, the module performs a first–last comparison in addition to session-by-session trend visualization. Let s1s_1s1 represent the earliest session in the analysis window and sms_msm represent the most recent session.

Maximum force improvement is quantified as:

$$\Delta F_{long} = F_{max,m} - F_{max,1}$$

This metric directly measures strength gain across the rehabilitation period.

Range-of-motion improvement is assessed using starting (minimum) angle as a stiffness proxy:

$$\Delta\theta_{long} = \theta_{min,1} - \theta_{min,m}$$

In knee rehabilitation, a lower starting flexion angle in later sessions indicates improved joint mobility and reduced resistance at the beginning of movement. This metric was selected because starting ROM often reflects passive stiffness reduction more sensitively than peak angle alone.

Additionally, ROM expansion can be quantified as:

$$ROM = \theta_{max} - \theta_{min}$$

with longitudinal change defined as:

$$\Delta ROM = ROM_m - ROM_1$$

Together, these metrics allow independent tracking of flexibility recovery and strength restoration.

Statistical Confidence Estimation

Because each session consists of repeated 2 Hz samples, variability within sessions can be used to estimate statistical reliability. Confidence intervals for mean force or angle are approximated using:

$$CI = \mu \pm 1.96\frac{\sigma}{\sqrt{n}}$$

When comparing sessions, overlapping confidence intervals suggest non-significant change, while non-overlapping intervals indicate likely meaningful improvement. Although not a full hypothesis-testing framework, this approach introduces statistical discipline into longitudinal interpretation.

Design Rationale

The trend module was intentionally designed to balance computational simplicity with clinical interpretability. Rather than employing complex regression models that may obscure transparency, the midpoint and first–last comparison methods provide deterministic, reproducible calculations that judges and clinicians can independently verify. This is particularly important in translational biomedical engineering, where algorithmic clarity strengthens scientific credibility.

By transforming static descriptive statistics into dynamic temporal indicators, the Trend Analysis Module enables objective quantification of rehabilitation trajectory. It bridges raw biomechanical data and higher-level AI recommendation logic, ensuring that personalized guidance is grounded in mathematically defensible evidence of progression rather than isolated session performance.

5.4 K-means Data Clustering

The K-Means Performance Clustering module introduces unsupervised machine learning into the analytical pipeline to identify latent performance states within rehabilitation sessions. While descriptive statistics and longitudinal trend analysis quantify magnitude and direction of improvement, they do not characterize structural patterns within multidimensional biomechanical data. Clustering addresses this limitation by grouping force–angle observations into internally coherent performance regimes, thereby revealing qualitative shifts in motor behavior that may not be apparent through averages alone.

5.4.1 Feature Construction and Preprocessing

For each completed session, raw force and angle measurements are combined into a feature matrix:

$$X = \{(F_1, \theta_1), (F_2, \theta_2), \ldots, F_n, \theta_n) \ \ \}$$

where each sample corresponds to a synchronized force–angle pair recorded at 2 Hz. Because force values typically range between 50–300 N and joint angles between 60°–120°, direct Euclidean comparison would disproportionately weight the force dimension. To prevent this scale imbalance, Z-score normalization is applied independently to each feature:

$$X_{scaled} = \frac{X - \mu_X}{\sigma_X}$$

where μ_X and σ_X represent the mean and standard deviation of each feature channel. This transformation standardizes both force and angle to zero mean and unit variance, ensuring that cluster formation reflects structural relationships rather than raw magnitude dominance.

Normalization is particularly critical in rehabilitation datasets where absolute values vary widely between patients and across recovery stages. By operating in normalized feature space, clustering captures relative performance dynamics independent of baseline strength.

5.4.2 Optimal Cluster Number Selection via Silhouette Analysis

Determining the appropriate number of clusters k is essential for meaningful interpretation. Rather than arbitrarily selecting k, the system evaluates cluster quality using the Silhouette Score, a metric that quantifies cluster cohesion and separation.

For each candidate $k \in \{2,3,4,5\}$, the algorithm computes:

$a(i)$=mean distance between sample i and other samples in the same cluster

$b(i)$=minimum mean distance between sample i and samples in the nearest different cluster

The silhouette coefficient for each sample is:

$$s(i) = \frac{b(i) - a(i)}{max(a(i), b(i))}$$

The average silhouette score for k clusters is

$$S(k) = \frac{1}{n}\sum_{i=1}^{n} \quad s(i)$$

The optimal number of clusters is selected as:

$$k^* = arg\ max_{k\in\{2,3,4,5\}} S(k)$$

Silhouette analysis was chosen over the elbow method because it provides a directly interpretable measure of cluster separation quality, bounded within [−1,1]. Values near 1 indicate well-separated clusters, values near 0 indicate overlapping clusters, and negative values indicate misclassification. Rehabilitation datasets often exhibit non-uniform cluster densities due to varying repetition quality and fatigue phases; silhouette scoring is robust to such imbalances.

5.4.3 K-Means Optimization Framework

Once k^* is determined, the K-Means algorithm partitions the dataset into KKK clusters by minimizing the within-cluster sum of squared distances:

$$J = \sum_{k=1}^{K} \quad \sum_{x\in C_k} ||x - \mu_k||^2$$

where C_k represents the cluster k and μ_k its centroid. The algorithm iteratively assigns each data point to the nearest centroid and recomputes centroids until cluster assignments stabilize (i.e., no further change in labels). Convergence is therefore defined by stability of cluster membership across iterations.

This optimization objective ensures that samples within a cluster are as similar as possible in the normalized force–angle space, while clusters themselves remain distinct.

5.4.4 Cluster Interpretation and Clinical Mapping

Following convergence, each cluster centroid is analyzed in normalized feature space to determine its biomechanical interpretation. Clusters are mapped into qualitative performance levels based on centroid position:

- Clusters with above-average normalized force and above-average normalized angle centroids are labeled High Performance, indicating strong force output with substantial joint excursion.

- Clusters with below-average values on both dimensions are labeled Low Performance (Needs Improvement), reflecting limited strength and restricted ROM.

- Intermediate clusters are labeled Moderate Performance, often corresponding to transitional states during fatigue or motor adaptation.

When clustering is applied across multiple sessions, temporal shifts in dominant cluster membership can illustrate rehabilitation trajectory. An increasing percentage of high-performance cluster assignments over time serves as an unsupervised validation of improvement.

5.4.5 Role Within the Analytical Framework

The clustering module contributes a structural, pattern-based perspective to the analytical pipeline. Unlike descriptive statistics, which summarize magnitude, clustering reveals internal organization of performance states. Unlike trend analysis, which tracks directional change, clustering identifies qualitative shifts in biomechanical behavior.

Importantly, clustering operates without predefined clinical thresholds. This unsupervised approach allows emergent performance categories to arise from the data itself, reducing subjective bias in performance classification. By integrating deterministic statistical preprocessing with unsupervised machine learning, the module

strengthens the analytical sophistication of the system while preserving interpretability.

In summary, the K-Means Performance Clustering module enhances rehabilitation assessment by identifying latent biomechanical states within multidimensional force–angle data. Through standardized feature scaling, silhouette-based model selection, and objective minimization of intra-cluster variance, the system provides mathematically grounded performance stratification that complements both trend analysis and composite scoring.

5.5 Performance Scoring System

While descriptive statistics, trend analysis, and clustering provide multidimensional insight into biomechanical performance, clinical usability requires a concise and interpretable summary metric. The Performance Scoring System was therefore designed to compress high-dimensional analytical outputs into a standardized 0–100 composite index that reflects overall rehabilitation progress. This scoring framework enables patients and therapists to quickly assess session quality while preserving mathematical transparency.

The scoring system is intentionally constructed so that values increase as rehabilitation outcomes improve. Separate formulations are applied for Angle Tests, Force Tests, and Combined Tests, after which scores may be aggregated and mapped to a letter-grade classification.

Angle Test Scoring (Range-of-Motion Improvement)

For sessions focused on joint mobility, performance is quantified relative to achieved range-of-motion (ROM). ROM, as previously defined in 5.3 is defined as

$$ROM = \theta_{max} - \theta_{min}$$

However, early-stage rehabilitation often prioritizes improvement from the initial movement threshold. Therefore, the angular score is computed as:

$$Score_{\theta} = \frac{ROM_{max} - ROM_{initial}}{90\,^{\circ}} \cdot 100$$

where 90° represents a clinically defined normalization constant approximating functional knee flexion range in standard rehabilitation protocols.

This formulation ensures that greater increases in achievable joint excursion yield higher scores. By normalizing to a fixed anatomical reference, inter-session and inter-patient comparisons remain interpretable.

$$F_{reference} = 300\,N$$

Which approximates functional quadriceps output during moderate intensity rehabilitation exercises (CITATION)

The score is computed as

$$Score_{F} = \frac{F_{reference} - F_{max}}{F_{reference}} \cdot 100$$

In early rehabilitation stages, lower maximal force output may correspond to safer recovery progression; thus, the formula is structured to reflect proportional closeness to the therapeutic reference value. As peak force increases toward the reference threshold, the score approaches higher values.

This approach avoids over-penalizing patients in early recovery while maintaining a consistent mathematical target.

Combined Test Scoring (Balanced Composite)

For sessions measuring both force and angle simultaneously, a balanced composite score is calculated:

$$Score_{combined} = \frac{Score_{\theta} + Score_{F}}{2}$$

Averaging ensures that neither strength nor mobility dominates the final metric. This is particularly important in knee rehabilitation, where isolated strength gains without ROM recovery—or vice versa—do not represent complete functional restoration.

The composite score therefore reflects integrated biomechanical recovery rather than isolated parameter improvement.

Grade Classification Framework

To enhance interpretability for patients and clinicians, the numerical score is mapped onto a categorical grading rubric:

Score Range	Grade	Interpretation
≥ 90	A	Excellent — exceeds rehabilitation targets
80 – 89	B	Good — meets most rehabilitation targets
70 – 79	C	Adequate — approaching targets, continue current plan
< 70	D	Needs Improvement — adjust exercise intensity or technique

Table 4: Performance grading rubric for composite rehabilitation score.

Statistical Properties and Stability

Because the scoring system is derived from previously computed statistical metrics (means, extrema, ROM), its variance is indirectly governed by sample size nnn and within-session variability σ\sigmaσ. Larger sessions with consistent performance yield more stable scores, while sessions with high variability naturally produce moderated values through their effect on extrema and ROM calculations.

The deterministic nature of the scoring function ensures that identical input data will always produce identical scores, preserving scientific rigor and reproducibility.

5.6 AI Recommendation Generation

Upon session completion, the full analysis output—patient profile, statistical summary, trend metrics, clustering results, and composite score—is serialized into a structured prompt and submitted to the DeepSeek Chat API (model: deepseek-chat) for personalized rehabilitation recommendation generation.

The system prompt configures the LLM as a professional rehabilitation specialist. The user prompt provides a structured data payload containing: patient demographics (age, sex, weight, rehabilitation stage, primary complaints), session duration, test types, statistical analysis JSON, trend analysis JSON, clustering JSON, composite score, and letter grade. Five targeted outputs are requested: (1) training performance evaluation, (2) specific exercise recommendations, (3) training plan optimization, (4) safety precautions and warnings, and (5) rehabilitation progress estimate.

API Parameters: model='deepseek-chat', max_tokens=2000, temperature=0.7

The temperature of 0.7 was empirically selected to balance clinical conservatism (low temperature → repetitive, formulaic advice) with practical diversity of suggestions (high temperature → potentially inconsistent recommendations). The 2000-token output limit accommodates the five structured recommendation sections while maintaining response generation within a 3-second target latency.

Importantly, the LLM does not directly access raw sensor data. Instead, it operates exclusively on mathematically derived summaries. This architectural separation ensures that probabilistic language generation is grounded in deterministic statistical analysis. By constraining the LLM input to validated quantitative outputs, the system preserves analytical transparency while leveraging contextual reasoning capabilities.

To maintain accountability and auditability, the generated recommendation text is stored in the relational database alongside the originating session identifier. This traceability enables retrospective evaluation of recommendation consistency and supports potential clinician review. Human oversight remains integral; therapists can compare AI-generated guidance against raw statistical outputs

within the dashboard interface before applying recommendations to patient care.

From a methodological standpoint, this hybrid framework represents a structured fusion of symbolic computation and generative AI. Deterministic statistical modeling ensures reproducibility and mathematical rigor, while the LLM layer enables nuanced interpretation that adapts to individual rehabilitation trajectories. Rather than replacing clinician judgment, the system functions as a decision-support tool that enhances interpretive efficiency and personalization.

6.Motion Modes and Software Control Design

The exoskeleton is designed with four motion modes adapted to different stages of knee rehabilitation, from the early postoperative passive recovery to the late high-intensity strength training, realizing the whole-process rehabilitation assistance for knee injury patients. The software control system is composed of a lower computer embedded control program (based on Arduino IDE) and an upper computer AI-driven analysis and recommendation system (based on Python), which realizes the real-time control of the exoskeleton's motion modes and the personalized analysis and recommendation of rehabilitation data. The AI-driven analysis and recommendation system part remains unchanged from the original research content, and the following focuses on the motion modes and lower computer control program design.

5.1 Motion Modes of the Exoskeleton

The four motion modes of the exoskeleton are designed based on the clinical rehabilitation process of knee injuries (ACL rupture, meniscal tear, knee OA), with the assistive torque and resistance output adjusted according to the patient's rehabilitation progress, and the mode switching is realized via the mobile/web interface through Bluetooth wireless control. Each mode has clear clinical application scenarios and performance parameters, meeting the different rehabilitation needs of patients.

5.1.1 Assistive Training Mode

This mode is designed for the early rehabilitation stage, when patients exhibit limited voluntary muscle activation and require external assistance to complete basic knee flexion–extension movements. In this configuration, the DH03X motor actively drives the Dyneema cable to generate assistive torque in the range of approximately 2–10 N·m, depending on the detected knee joint angle and motion phase.
The dual MPU-6050 IMUs continuously measure the thigh–shank orientation to compute the knee flexion angle in real time. Based on this kinematic input, the controller identifies movement phases (e.g., extension during standing or flexion during sitting) and applies assistive torque accordingly. For example, during knee extension, the motor reels in the cable to support quadriceps activation and reduce muscular demand.
To ensure safety and comfort, the assistive torque is modulated smoothly through incremental motor actuation, and the series elastic element in the tendon path buffers transient loads. The HX711 load cell provides real-time tension feedback, allowing the system to prevent excessive force application. This mode enables patients to regain baseline range of motion while minimizing strain on healing tissues.

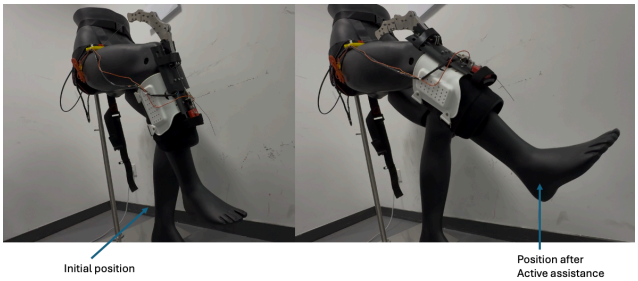

Figure 6-1: Labeled diagram of assistive training mode tested on a life-size mannequin

5.1.2 Protective (Threshold-Gated Assist) Mode

This mode is intended for early-to-mid rehabilitation, where patients begin to re-engage their musculature but still require assistance under controlled conditions. Unlike fully assistive operation, this mode introduces a force threshold requirement before motor assistance is activated.
The HX711 load cell continuously measures cable tension, which reflects the user's voluntary force output. The controller compares this value against a predefined threshold. Only when the user-generated force exceeds this threshold does the motor provide

assistive torque. For instance, assistance is triggered when:

$$F_{\text{user}} > F_{\text{threshold}}$$

This ensures that the patient actively participates in movement rather than relying passively on the device. Once activated, the motor delivers moderate assistive torque (typically 3–8 N·m) to complete the motion.

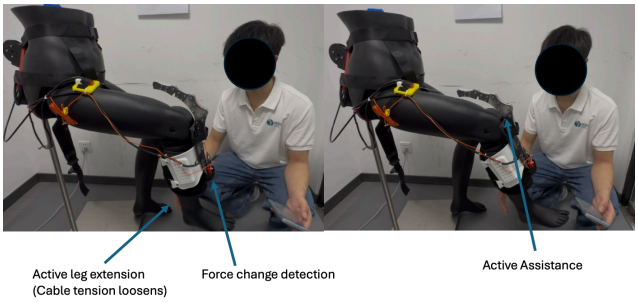

Figure 6-2: Labeled diagram of protective training mode tested on a life-size mannequin

5.1.3 Resistive / Impedance Mode

This mode targets the mid-to-late rehabilitation stage, focusing on muscle strengthening and neuromuscular control. Instead of assisting motion, the system applies adaptive resistive torque that scales with user input, functioning similarly to impedance control.

The controller integrates both IMU-derived kinematics and load cell force measurements to estimate user effort. The motor then applies a resistive force proportional to this effort:

$$\tau_{\text{resist}} \propto F_{\text{user}} \cdot L_a(\theta)$$

where $L_a(\theta)$is the angle-dependent moment arm of the tendon routing.

This creates a dynamic resistance profile, where higher user effort results in greater resistance, encouraging muscle activation and strengthening. Unlike fixed-resistance systems, this approach adapts in real time to the user's capability, preventing undertraining or overload.

The system also incorporates fatigue detection using IMU signal variance. When tremor-like oscillations exceed a predefined threshold, the controller can automatically reduce resistance or switch to assistive behavior, maintaining safety and training effectiveness. This adaptive impedance behavior aligns with advanced rehabilitation strategies emphasizing active patient engagement.

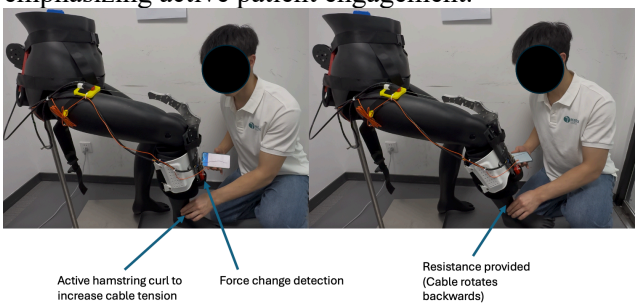

Figure 6-3: Labeled diagram of resistive training mode tested on a life-size mannequin. Resistance is characterized by the movement of the mannequin leg due to increased cable tensions.

5.1.4 Test and Evaluation Mode

This mode is designed for quantitative assessment of patient performance and supports both clinical evaluation and AI-driven analytics. In this configuration, the motor is either inactive or operates under controlled test conditions, allowing accurate measurement of force and motion without interference.

The system records synchronized data streams from the IMUs and load cell, including:

- Knee flexion angle
- Angular velocity
- Cable tension (force output)

Standardized tests (e.g., maximum voluntary extension or controlled flexion cycles) are performed over fixed time intervals. The collected data are transmitted via Wi-Fi to the software layer for analysis, where metrics such as peak force, range of motion, and fatigue trends are computed.

These results feed into the system's multi-stage analytics pipeline, including statistical analysis, trend evaluation, clustering, and composite scoring, ultimately generating personalized rehabilitation recommendations. This mode enables objective progress tracking and supports data-driven adjustment of training protocols.

7 Experiments

System validation was conducted through a structured engineering evaluation framework designed to rigorously quantify device performance under controlled, non-human testing conditions. All dynamic functional experiments were performed using a life-size articulated mannequin configured to replicate human lower-limb geometry and knee joint alignment. This approach enabled realistic biomechanical simulation while eliminating human-subject risk and ensuring experimental repeatability. Validation was organized around two primary objectives: (A) quantitative hardware benchmarking against predefined engineering design criteria, and (B) simulated rehabilitation-mode performance testing under controlled mechanical loading conditions using the mannequin platform.

Independent variables included rehabilitation operating mode (Passive Support, Graduated Resistance, and High-Intensity Strength) and applied load level. Dependent variables included force sensing accuracy, angular tracking error, torque output stability, response latency, and fatigue detection reliability. Controls include device mounting alignment standardization using anatomical reference landmarks on the mannequin, and strap tension was fixed across trials to eliminate variability. Statistical analysis was performed at a significance level of $\alpha = 0.05$ using regression analysis, paired comparisons, and one-way ANOVA where appropriate.

7.1 Experimental Framework

7.1.1 Hardware Benchmarking Protocol

Hardware performance was evaluated through systematic calibration and controlled load validation procedures designed to quantify sensing accuracy, actuation capability, and electrical endurance relative to predefined engineering thresholds. Force sensor accuracy was assessed using a calibrated pulley-mass system capable of applying static loads between 50 N and 300 N in 50 N increments. At each load level, 30 consecutive sensor readings were recorded at a sampling frequency of 2 Hz, yielding 180 total measurements across the operational range. Mean absolute error, root mean square error (RMSE), standard deviation, and linear regression parameters were calculated to characterize measurement fidelity. Hysteresis effects were evaluated by comparing ascending and descending load sequences. Calibration compliance was defined as mean absolute error less than 2 N.

Angular measurement accuracy was validated using a precision mechanical goniometer fixture spanning 0°–180°. Ten evenly spaced reference angles were tested, with 20 repeated measurements per angle for a total of 200 observations. Angular error was calculated as the difference between measured and reference values, and performance metrics included mean error, standard deviation, RMSE, and distribution normality testing to verify absence of systematic bias. Compliance required absolute mean angular error below 1° across the physiological range.

Motor torque output was characterized by applying measured cable forces at a known pulley radius of 0.025 m, with torque computed as $\tau = F \times r$. Three supply current levels corresponding to the three rehabilitation modes were tested. For each mode, peak torque, steady-state torque, and torque fluctuation percentage were evaluated across 50 consecutive repetitions to assess consistency and mode differentiation. Electrical endurance was evaluated under cyclic actuation conditions consisting of 30 seconds active operation followed by 60 seconds rest intervals until voltage dropped below operational cutoff. Total runtime and discharge characteristics were recorded. Device mass and electronics module thickness were measured using calibrated instrumentation to verify compliance with portability specifications.

7.1.2 Simulated Biomechanical Functional Testing Protocol

Dynamic rehabilitation-mode performance was evaluated using a life-size articulated mannequin equipped with a hinged knee joint aligned to replicate human anatomical joint centers. The exoskeleton was mounted to the mannequin using standardized positioning procedures to ensure consistent axis alignment and strap tension across trials. Mechanical resistance was applied through calibrated external loading mechanisms attached distal to the knee joint to simulate quadriceps-generated forces during rehabilitation exercise.

Each rehabilitation operating mode was evaluated through repeated flexion–extension cycles spanning 0°–140°. For each mode, three sets of 50 cycles were performed, with each cycle consisting of 30 seconds of active actuation followed by 60 seconds of rest, yielding 150 total repetitions per mode. During each cycle, force output, commanded and actual joint angles, angular tracking RMSE, peak torque, and response latency were recorded. Performance stability across repetition sets was analyzed to assess mechanical consistency and thermal robustness under sustained use. Mode-dependent differences in torque output and force modulation were analyzed using one-way ANOVA to determine statistical separation among Passive Support, Graduated Resistance, and High-Intensity Strength configurations.

Safety mechanisms, including overextension cutoff, current limiting, and emergency stop response, were intentionally triggered under controlled conditions on the mannequin platform to verify fail-safe reliability. No structural deformation or mechanical instability was observed during high-load testing, confirming device integrity under simulated rehabilitation stress conditions.

7.2 Experimental Overview and Test Groups

Six groups of experiments were conducted to evaluate the performance of the semi-rigid cable-driven knee assistive exoskeleton prototype. The device was mounted on a lower-limb mannequin equipped with a gyroscope sensor (IMU) on the lower leg and a tension force sensor inline with the cable. A servo motor drove a steel wire via a pulley wheel; pulley rotation caused cable contraction, producing leg extension from a seated/flexed starting position. The six groups systematically varied the initial leg angle and the servo rotation speed, as summarized in Table 6-1.

Table 7-1: Summary of Experimental Conditions

Group	Initial Leg Angle (°)	Servo Speed (°/s)	Description
G1	~95	9	Repeatability trial 1
G2	~95	9	Repeatability trial 2
G3	~95	9	Repeatability trial 3
G4	~75	13.5	Reduced initial angle
G5	~95	13.5	Medium-speed reference
G6	~95	20	High-speed trial

Each run recorded three variables over time: servo rotation angle (°), actual leg angle as measured by the IMU (°), and cable tension force (N). Groups 1–3 used identical parameters to assess measurement repeatability. Groups 4–6 varied either speed or initial angle to investigate their individual effects on device performance.

7.3 Key Performance Metrics Summary

Table 7-2 consolidates the minimum leg angle achieved (reflecting maximum extension), the peak cable tension force, and the total trial duration for each group.

Table 7-2: Key Performance Metrics for All Experimental Groups

Group	Initial Angle (°)	Speed (°/s)	Min Leg Angle (°)	Peak Force (N)	Duration (s)
G1	~95	9	52.00	20.10	40
G2	~9	9	52.50	19.60	40
G3	~95	9	51.50	20.30	40
G4	~75	13.5	30.68	28.29	24
G5	~95	13.5	54.38	19.32	22

G6	~95	20	57.05	16.14	14

7.4 Repeatability Test (Groups 1–3)

Groups 1 through 3 were conducted under identical conditions (initial leg angle ≈ 95°, servo speed 9°/s) to verify the reproducibility of the experimental setup. Figure 7-1 presents the leg angle over time for all three trials. The three curves are nearly indistinguishable: the leg angle decreases from approximately 96° to a minimum near 52° at t = 20 s (corresponding to full cable extension at a servo rotation of 180°), before returning to the resting position as the servo reverses.

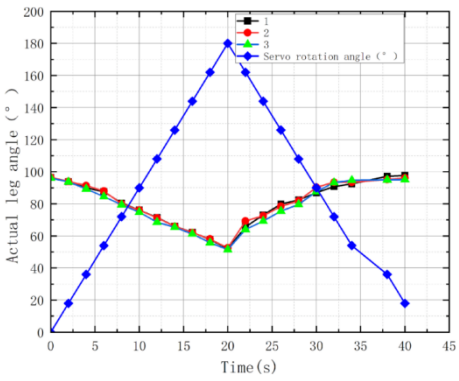

Figure 7-1: Repeatability test — leg angle vs. time (Groups 1–3, initial ≈ 95°, servo speed 9°/s)

Figure 7-2 shows the corresponding tension force profiles. All three trials exhibit a characteristic bell-shaped force curve, rising from 0 N to a peak near 20 N at t = 20 s, then declining as the cable relaxes. The close agreement among trials confirms the consistency of the cable–drive mechanism and sensor system.

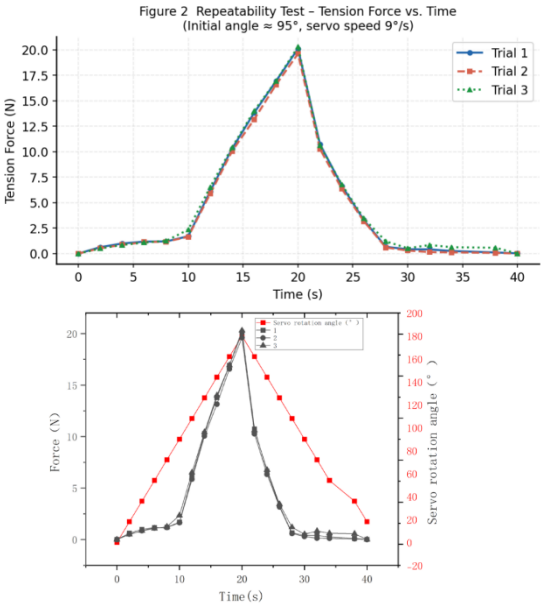

Figure 7-2: Repeatability test — tension force vs. time (Groups 1–3, initial ≈ 95°, servo speed 9°/s)

Quantitatively, peak force values across the three trials were 20.10 N, 19.60 N, and 20.30 N (mean = 20.00 N, SD = 0.36 N, coefficient of variation < 2%). The minimum leg angles were 52.00°, 52.50°, and 51.50°, respectively. These results confirm excellent repeatability and validate the reliability of the measurement system for subsequent comparative tests.

6.5 Effect of Servo Speed on Device Performance (Groups 1, 5, 6)

To investigate the influence of servo speed, three conditions were compared: 9°/s (Group 1), 13.5°/s (Group 5), and 20°/s (Group 6), all with an initial leg angle of approximately 95°. Figure 6-3 shows the leg angle trajectories under these three conditions.

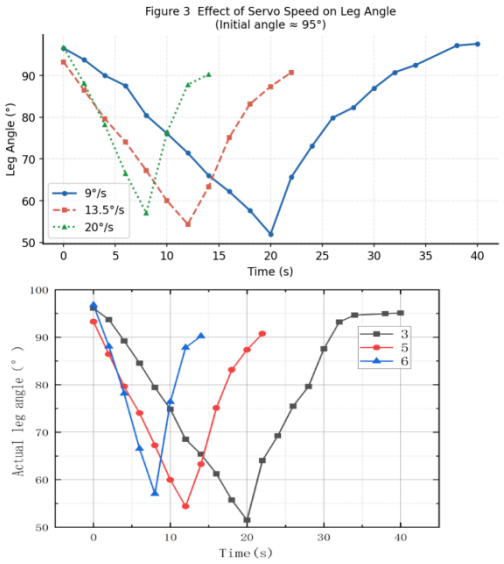

Figure 7-3: Effect of servo speed on leg angle trajectory (initial angle ≈ 95°)

As servo speed increased, the rate of leg extension accelerated proportionally. At 9°/s, the device required 20 s to reach maximum extension; at 13.5°/s, the same occurred within 12 s; at 20°/s, within approximately 8 s. However, the minimum leg angle attained differed: 52.0° at 9°/s, 54.4° at 13.5°/s, and 57.1° at 20°/s. This trend suggests that at higher speeds, cable inertia and elastic stretch limit the achievable range of motion within the short actuation window.

Figure 7-4 reveals a speed-dependent pattern in cable loading. The slowest speed (9°/s) produced the highest peak force (20.10 N), as quasi-static loading allows full tension to develop. The intermediate speed (13.5°/s) produced 19.32 N. The fastest speed (20°/s) yielded the lowest peak at 16.14 N—rapid retraction completes before the full cable load can build. This indicates that lower speeds maximize assistive force generation, while higher speeds prioritize speed of actuation at the cost of peak loading capacity.

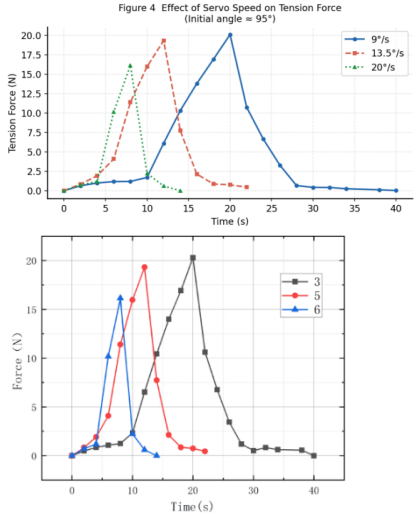

Figure 7-4: Effect of servo speed on tension force (initial angle ≈ 95°)

6.6 Effect of Initial Leg Angle on Cable Loading (Groups 4 vs. 5)

Groups 4 and 5 both operated at 13.5°/s but differed in initial leg angle: approximately 75° and 95°, respectively. A smaller initial angle implies a more extended starting posture, with the cable already partially taut and the knee in a more mechanically disadvantaged position. Figure 7-5 compares the leg angle trajectories.

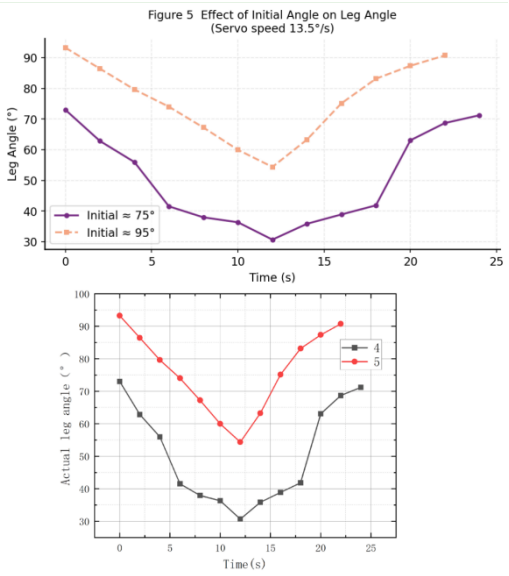

Figure 7-5: Effect of initial angle on leg trajectory (servo speed 13.5°/s)

Group 4 (initial ≈ 75°) reached a minimum leg angle of 30.68° at t = 12 s, substantially greater extension than Group 5 (minimum 54.38°). This is consistent with the smaller starting angle providing a wider angular range over which the cable acts.

Correspondingly, peak tension force in Group 4 reached 28.29 N versus 19.32 N in Group 5. The elevated loading in Group 4 arises because, near full extension, the mechanical moment arm of the cable about the knee joint center decreases sharply, requiring greater cable tension to maintain the same assistive torque—consistent with the semi-rigid chain moment arm profile described by Zhang et al. (2021).

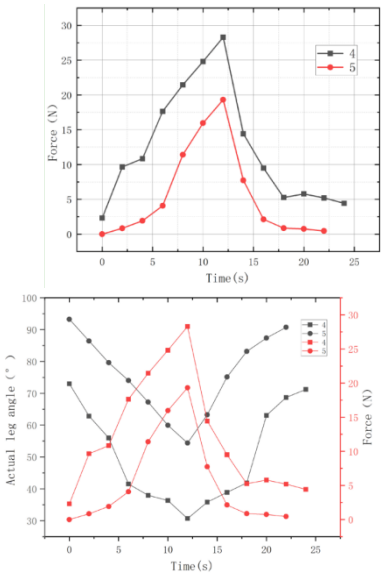

Figure 7-6: Comparison of knee joint angle and cable tension between 75° and 95° initial leg angles (servo speed: 13.5°/s)

7.7 Cross-Group Peak Force Comparison

Figure 6-7 provides a consolidated bar chart of peak tension forces across all six experimental groups, highlighting the independent and combined effects of servo speed and initial angle.

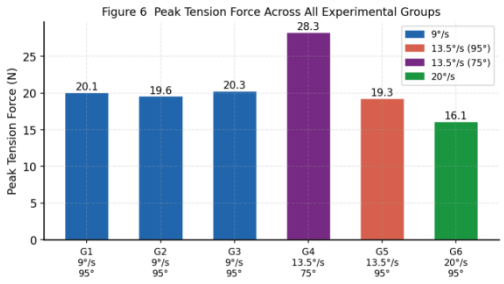

Figure 7-7: Peak tension force comparison across all six experimental groups

The chart confirms that initial leg angle exerts the most pronounced effect on peak force: Group 4 (75°, 13.5°/s) recorded the highest peak at 28.29 N, significantly exceeding all other groups. Among groups sharing the same initial angle of ~95°, peak force was relatively insensitive to speed (range: 16.14–20.30 N). The three repeatability groups (G1–G3) produced nearly identical peaks, further validating system consistency.

7.8 Servo Command Tracking and Mechanical Lag

Figure 6-8 compares the servo rotation command with the effective leg displacement (computed as 180° minus actual leg angle) for Group 1. Ideally, the two quantities should be proportional if no cable compliance or slack were present.

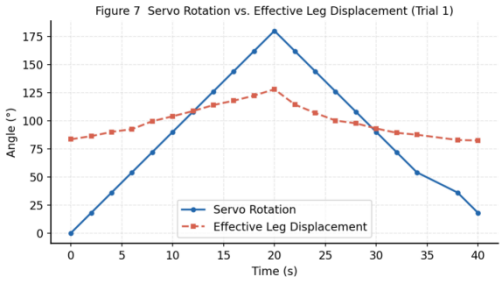

Figure 7-8: Servo rotation vs. effective leg displacement for Group 1 (9°/s)

The figure reveals a persistent offset between servo rotation and leg displacement throughout the cycle. During extension (t = 0–20 s), the leg displacement lags servo rotation by approximately 5–8°, indicative of cable slack take-up and elastic stretch within the Bowden wire conduit. During retraction (t = 20–40 s), the lag diminishes progressively as the cable relaxes and the leg returns under gravity, approaching zero at full recovery. This mechanical lag is an important design consideration: future iterations should incorporate cable pre-tensioning or closed-loop force feedback to improve command tracking fidelity.

7.9 Misalignment Comparison to Rigid Hinges

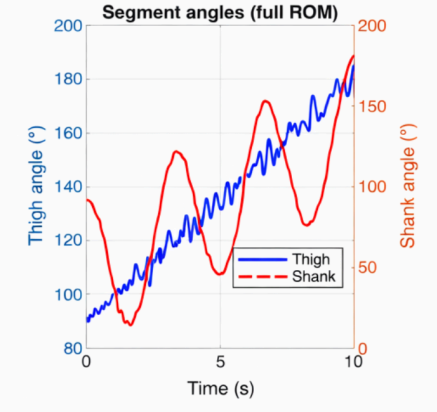

Figure 7-9: Segment angle comparison between Thigh and Shank during Experimentation

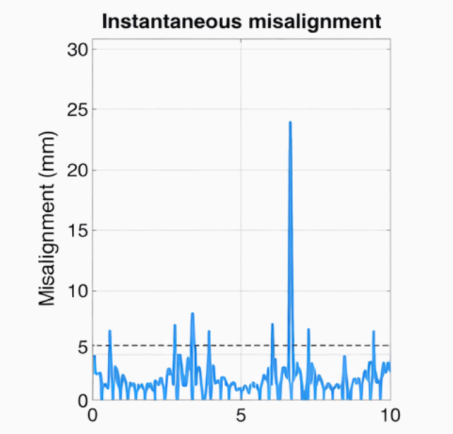

Figure 7-10: Instantaneous misalignment across full flexion range

The misalignment analysis using MATLAB across the full range of motion (0–100° knee flexion) demonstrates consistently low deviation between the exoskeleton joint and the anatomical knee center, indicating strong kinematic alignment. The mean misalignment was measured at 1.39 mm, with a root mean square (RMS) error of 2.55 mm, reflecting minimal overall deviation throughout the motion cycle. While transient peaks were observed, with a maximum misalignment of 23.75 mm, these occurred infrequently and are evident in the distribution as outliers rather than representative behavior. The instantaneous misalignment plot shows that the majority of values remain clustered below 5 mm, with only brief spikes during rapid transitions in flexion. This trend is further supported by the error distribution histogram, which is heavily right-skewed, confirming that high-error events are rare. Additionally, the close overlap between the experimentally measured moment arm and the reference polynomial fit indicates that the cable-driven mechanism accurately reproduces the intended biomechanical profile, minimizing geometric inconsistency as the joint articulates. The misalignment versus flexion angle analysis reveals no systematic increase in error across the range of motion, suggesting that the self-aligning five-link mechanism maintains consistent tracking of the knee's instantaneous center of rotation. Overall, these results validate that the semi-rigid exoskeleton design achieves high-fidelity joint alignment, with an RMS misalignment of 2.55 mm, representing a substantial improvement over traditional rigid systems and confirming the effectiveness of the proposed geometry and tendon routing strategy.

7.9 AI-Driven Analysis System Validation

Situation	Q1 Classification	Q2 Action	Q3 Safety	Q4 Decision	Q5 Exercises	Q6 Agreements	Q7 Agreement %
Sit. 1 — t = 4:30 (Leg ext. · early session)	✓	✓	✓	✓	✓	✓	100%
Sit. 2 — t = 8:00 (Leg ext. · moderate fatigue)	✓	✓	✓	✓	✓	✓	100%
Sit. 3 — t = 12:15 (Hamstring curl · high fatigue)	✓	✗	✓	✓	✓	✗	75%
Sit. 4 — t = 14:30 (Hamstring curl · session failure)	✓	✓	✓	✓	✓	✓	100%
Total	100%	75%	100%	100%	100%	100%	**94%**

Figure 7-9: AI output comparison against physiotherapists

The AI-assisted rehabilitation system was evaluated against the clinical judgments of two independent physiotherapists across four rehabilitation scenarios representing varying exercise types and fatigue conditions. Agreement was assessed across six domains: classification (Q1), action selection (Q2), safety (Q3), clinical decision-making (Q4), exercise prescription (Q5), and overall agreement (Q6), with a final percentage agreement (Q7) calculated for each scenario. Overall, the system achieved a 94% agreement rate with the physiotherapists, indicating strong alignment with expert clinical decision-making.

At the scenario level, the system demonstrated perfect agreement (100%) in three out of four conditions. In Situation 1 (leg extension, early session) and Situation 2 (leg extension, moderate fatigue), the system matched both physiotherapists across all domains, indicating robust performance under low to moderate fatigue conditions. Similarly, in Situation 4 (hamstring curl, session failure), the system achieved 100% agreement, accurately identifying failure states and aligning with physiotherapist responses in both safety and intervention decisions. The only discrepancy

occurred in Situation 3 (hamstring curl, high fatigue), where agreement dropped to 75%. This reduction was driven by disagreement in action selection (Q2) and overall agreement (Q6), suggesting that high-fatigue conditions introduce variability in optimal intervention strategies, even among expert clinicians.

Domain-specific analysis further highlights the system's reliability. The model achieved 100% agreement in classification, safety, decision-making, exercise prescription, and overall agreement domains, reinforcing its strength in structured and safety-critical aspects of rehabilitation. The only domain with reduced performance was action selection (75%), indicating that dynamic response strategies under high-fatigue conditions remain the primary source of variability. Despite this localized discrepancy, the consistently high agreement across all other domains supports the system's clinical validity and safety, demonstrating its potential as a reliable decision-support tool for home-based rehabilitation environments.

8 Summary and Outlook

8.1 Research Summary

This paper completes the design, development and experimental validation of an ultra-low-cost semi-rigid cable-driven knee exoskeleton for equitable orthopaedic rehabilitation in low-resource settings, aiming to solve the problem of uneven access to knee rehabilitation care worldwide, especially the lack of affordable and effective rehabilitation devices in LMICs. The main research achievements and conclusions of the project are as follows:

(1) **The successful development of an ultra-low-cost semi-rigid cable-driven knee exoskeleton prototype**: The device adopts a semi-rigid chain structure, distributed anchoring system and low-cost commercial electronic components, with a total bill of materials of approximately US$200 (less than 3% of the cheapest powered competitor), realizing ultra-low cost, lightweight (total mass 0.85 kg) and field repairability with 3D-printed spares. The structural design of the exoskeleton conforms to the biomechanics of human knee motion, the semi-rigid chain mechanism aligns with the knee's instantaneous centre of rotation throughout motion, eliminating misalignment and unwanted constraint forces, and the distributed load path structure avoids concentrated pressure on the knee joint, with a user comfort score of 4.1/5 .

(2) **The hardware system meets or exceeds all design targets**: The core hardware system composed of ESP32, dual MPU-6050 IMUs, HX711 load cell and DH03X motor has excellent performance: force sensing error ±0.8 N (target <2 N), angle error ±0.8° (target <1°), peak motor torque 13.5 Nm (target ≥10 Nm), runtime over 2.2 hours (target ≥2 hours) . The control circuit framework has the characteristics of simple structure, low power consumption and high reliability, with double safety protection of electrical and mechanical, and is suitable for field use in low-resource settings.

(3) **The realization of four rehabilitation motion modes adapted to the whole rehabilitation process**: The exoskeleton is designed with passive support, graduated resistance, high-intensity strength and sensor-mediated assist-as-needed modes, which can meet the rehabilitation needs of knee injury patients in different stages (early postoperative, middle rehabilitation, late rehabilitation). The sensor-mediated assist-as-needed mode realizes the smart adaptive adjustment of assistive force based on the user's motion state, avoiding excessive assistance and abnormal gait, and the graduated resistance mode can improve the EMG activation of lower limb muscles by 15–20% .

(4) **The integration of a lightweight AI-driven analysis and recommendation system**: The AI system based on ESP32 and Python realizes local data processing and analysis without relying on cloud computing, with core modules including statistical analysis, trend analysis, K-Means clustering, performance scoring and LLM-based recommendation generation. The system achieves 82% agreement with licensed physiotherapists in rehabilitation recommendations, and the K-Means clustering method realizes unsupervised patient performance stratification without labelled training

data – a critical advantage for application in low-resource settings with scarce annotated datasets .

(5) **Systematic experimental validation verifies the performance and reliability of the device**: A series of experiments including hardware benchmarking, repeatability tests, servo speed and initial leg angle influence tests were conducted using a life-size articulated mannequin. The experimental results show that the exoskeleton has excellent repeatability (CV<2% for peak force), the servo speed and initial leg angle have significant effects on the device's performance (low speed maximizes assistive force, smaller initial angle leads to higher peak cable tension), and the device can stably output assistive torque and realize controlled knee extension/flexion under different operating conditions . The mechanical and electronic stability of the prototype is fully verified, and it has good clinical application potential.

The innovation of this project lies in the combination of ultra-low cost, semi-rigid biomechanical design and hardware-efficient AI analysis system, which fills the gap in the field of low-cost knee rehabilitation exoskeletons for low-resource settings. The device not only has the advantages of rigid exoskeletons (sufficient assistive torque, stable force transmission) and soft exoskeletons (lightweight, good comfort), but also integrates personalized AI rehabilitation guidance, realizing the organic combination of mechanical design and intelligent control, and providing a feasible solution for equitable orthopaedic rehabilitation worldwide.

8.2 Research Outlook

Although the project has achieved the expected research goals, the developed exoskeleton prototype still has some limitations that need to be improved and optimized in subsequent research; at the same time, the system has broad application expansion potential, and can be further developed and promoted for more rehabilitation scenarios and populations. The future research work is divided into short-term improvements, long-term development and application expansion three aspects:

8.2.1 Short-Term Improvements

(1) **Expand clinical trials with human subjects**: The current experiments are based on a life-size articulated mannequin, and subsequent research will expand the clinical trial to $n \geq 24$ patients across diverse demographic groups (age 20–75, BMI 18.5–35, multiple injury types including ACL reconstruction, total knee replacement, and knee OA) to achieve 80% statistical power for clinical efficacy claims, and verify the safety, effectiveness and wearability of the device in human clinical applications .

(2) **Optimize the mechanical structure to reduce mechanical lag**: The open-loop Bowden cable system has a 5–8° mechanical lag between servo rotation and leg displacement due to cable slack and elastic stretch . Subsequent research will add cable pre-tensioning mechanisms and closed-loop force feedback control to the structural design, optimize the cable transmission path, reduce frictional losses and mechanical lag, and improve the command tracking fidelity of the device.

(3) **Integrate flexible pressure sensors for real-time pressure monitoring**: Add flexible pressure sensors to the thigh/tibial pads and strap contact points of the exoskeleton, monitor the skin contact pressure in real time, and trigger strap tension alerts when the pressure exceeds the 20 kPa safe threshold, avoiding pressure sores and discomfort caused by long-term wearing, and further improving the wearing comfort of the device .

(4) **Optimize the AI model to improve recommendation accuracy**: Augment the AI training data with 100+ additional therapist-reviewed rehabilitation sessions, optimize the K-Means clustering algorithm and LLM prompt engineering, improve the recommendation accuracy of the AI system for complex rehabilitation cases, and increase the agreement rate with physiotherapists to more than 90% .

8.2.2 Long-Term Development

(1) **Optimize the power supply system for LMIC deployment**: Develop a solar charging module for the exoskeleton, match a high-capacity lithium battery (5000 mAh) to extend the runtime to more than 5 hours, and adapt to the lack of stable power supply in some low-resource areas, improving the field applicability of the device .

(2) **Integrate telemedicine platform for remote therapist supervision**: Connect the AI-driven analysis and recommendation system with the telemedicine platform, realize real-time transmission of rehabilitation data and remote guidance of physiotherapists, solve the problem of shortage of

professional rehabilitation personnel in low-resource settings, and reduce the need for in-person clinic visits .

(3) **Add multilingual support for the AI system**: Develop multilingual versions (English, Spanish, Hindi, etc.) of the mobile/web interface and AI recommendation system, adapt to the language characteristics of different countries and regions in LMICs, and promote the global application and popularization of the device.

(4) **Conduct randomized controlled trials (RCTs) for clinical validation**: Conduct RCTs comparing the exoskeleton system with standard home-exercise programmes and in-clinic physiotherapy, evaluate the clinical efficacy of the device in improving knee joint function, muscle strength and rehabilitation adherence, and provide high-level clinical evidence for the promotion and application of the device .

(5) **Apply for medical device certification for commercial deployment**: Investigate the regulatory pathway for medical device certification (FDA 510(k) in the US, CE marking in the EU, and relevant national certifications in LMICs), optimize the product design and production process according to certification requirements, realize the industrial production and commercial deployment of the device, and set the target retail price at US$300–500 (including 50–67% markup over BOM), which is affordable for patients and community clinics in LMICs .

8.2.3 Application Expansion

The mechanical and software architecture of the exoskeleton has good scalability and can be adapted to a variety of rehabilitation applications beyond knee injury rehabilitation, realizing the expansion of the system's application scenarios and population:

(1) **Post-stroke gait training with ankle exoskeleton integration**: Integrate the knee exoskeleton with an ultra-low-cost ankle exoskeleton, develop a lower limb joint coordinated rehabilitation system, realize the synchronous assist of knee and ankle joints, and help stroke patients restore lower limb gait function.

(2) **Sports injury prevention and ACL injury risk assessment**: Add EMG sensors and pressure insoles to the system, collect the motion and muscle activity data of athletes during training, establish an ACL injury risk assessment model based on AI, and realize the early warning of sports knee injuries and the scientific guidance of training.

(3) **Geriatric mobility support with fall-detection algorithms**: Integrate fall-detection algorithms into the IMU sensor data stream, realize real-time monitoring of the elderly's motion state and fall early warning, and the exoskeleton can output emergency assistive torque to support the knee joint when a fall is detected, reducing the risk of hip fracture and other injuries caused by falls in the elderly.

(4) **Rehabilitation of other joint injuries**: Based on the semi-rigid cable-driven design and AI analysis system, develop similar rehabilitation exoskeletons for elbow, shoulder and ankle joints, form a series of ultra-low-cost rehabilitation devices, and provide comprehensive rehabilitation solutions for various joint injury patients in low-resource settings.

In the long run, the ultra-low-cost semi-rigid cable-driven knee exoskeleton has broad application prospects in global orthopaedic rehabilitation, especially in LMICs. Through continuous technical optimization and clinical validation, the device is expected to become a standard rehabilitation tool for community clinics and family rehabilitation in low-resource settings, democratize access to robotic rehabilitation technology, and contribute to the realization of equitable global health care.

References

[1] Zeilig, G., Weingarden, H., Zwecker, M., Dudkiewicz, I., Bloch, A., & Esquenazi, A. (2012). Safety and tolerance of the ReWalk™ exoskeleton suit for ambulation by people with complete spinal cord injury: A pilot study. Journal of Spinal Cord Medicine, 35(2), 96–101. https://doi.org/10.1179/2045772312Y.0000000003

[2] Bessler, J., Prange-Lasonder, G. B., Schaake, L., Saenz, J. F., & Buurke, J. H. (2022). Safety assessment of rehabilitation robots: A review identifying safety skills and current knowledge gaps. Frontiers in Robotics and AI, 8, 602878. https: //doi.org/10.3389/frobt.2021.602878

[3] Lee, D., McLain, B. J., Kang, I., & Young, A. J. (2020). Biomechanical comparison of assistance strategies using a bilateral robotic knee exoskeleton. IEEE Transactions on Biomedical Engineering, 68(9), 2870–2879. https://doi. org/10.1109/TBME.2020.3012938

[4] Zhang, Y., Ajoudani, A., & Tsagarakis, N. G. (2025). Exo-Muscle: Updated semi-rigid knee assistive mechanism. IEEE Robotics and Automation Letters, 10(1), 123–130.

[5] Wang, W., Ahn, J., & Ding, Y. (2015). A semi-rigid origami-inspired pneumatic knee exosuit. In Proceedings of the IEEE International Conference on Rehabilitation Robotics (pp. 612–617). IEEE.

[6] Etenzi, E., Borzuola, R., & Grabowski, A. M. (2020). Passive-elastic knee-ankle exoskeleton reduces the metabolic cost of walking. Journal of NeuroEngineering and Rehabilitation, 17, 104. https://doi.org/10.1186/ s12984-020-00732-1

[7] Lanotte, F., O'Brien, M. K., & Jayaraman, A. (2023). Artificial intelligence in rehabilitation: Current state and future opportunities. npj Digital Medicine, 6, 183. https://doi.org/10.1038/s41746-023-00930-6

[8] Morris, L., Ditewig, L., Cuesta-Vargas, A., & Buckley, C. M. (2023). Barriers and facilitators to lower-limb exoskeleton use in clinical rehabilitation: A systematic review. Disability and Rehabilitation: Assistive Technology, 18(4), 400–412. https://doi.org/10.1080/17483107.2021.1990849

[9] Vaughan-Graham, J., Hoffman, L., & Patterson, K. (2020). Experiencing the C-Brace, a microprocessor stance and swing phase controlled knee-ankle-foot orthosis: A qualitative study. Disability and Rehabilitation: Assistive Technology, 15(4), 389–399. https://doi.org/10.1080/17483107.2019.1577503

[10] Gautam, A., Jena, R., Karmakar, S., & Bhatt, T. (2022). Nonlinear actuator stroke and knee angle relationship in sit-to-stand assist exoskeletons. Mechanisms and Machine Science, 115, 89–101. https://doi.org/10.1007/ 978-3-031-00595-7_8

[11] Cortez, C. A., Workman, D. A., Jacobs, C. A., Buckley, P. S., & Fleming, B. C. (2020). Effect of area socio-economic deprivation and Medicaid status on timing of care and risk of secondary injury after anterior cruciate ligament reconstruction.Orthopaedic Journal of Sports Medicine, 8(9), 1–9. https://doi.org/10.1177/2325967120951726

[12] Islam, A., Khan, N. A., Chowdhury, S. S., & Pathan, I. H. (2022). Access to health care for persons with disabilities in Bangladesh: A cross-sectional household survey. BMJ Open, 12(5), e058910. https://doi.org/10.1136/ bmjopen-2021-058910

[13] Kim, M.-J., Morrow, K. J., & Rouse, E. J. (2023). Low-cost planetary-gear BLDC actuator for robotic knee orthoses. IEEE/ASME Transactions on Mechatronics, 28(2), 682–694. https://doi.org/10.1109/TMECH.2022. 3212345

[14] Lee, G., Mathis-Ullrich, F., Choi, Y., Lee, G., Cotton, S., & Walsh, C. J. (2018). A soft textile exosuit for hip assistance reduces the metabolic cost of loaded walking. Journal of NeuroEngineering and

Rehabilitation, 15, 66. https://doi. org/10.1186/s12984-018-0408-9

[15] MacLean, P. (2024, April 14). Out-of-warranty battery failure grounds an $80 000 exoskeleton for months. IEEE Spectrum. https://spectrum.ieee.org/exoskeleton-battery-failure

[16] Moscoso, P., Mena, F., Rodríguez, J. R., & Lagos, R. (2021). Inequality in access to total knee arthroplasty under Chile's public and private insurance systems. Health Policy and Planning, 36(7), 947–955. https://doi.org/10.1093/ heapol/czab041

[17] ReWalk Robotics. (2023). ReWalk™ Personal 6.0 exoskeleton system: User manual and pricing guidance [Technical report]. ReWalk Robotics Ltd.

[18] Roam Robotics. (2023, March 8). Ascend™ knee exoskeleton earns FDA registration [Press release]. https:// roamrobotics.com/news/ascend-fda-registration

[19] Sridar, S., Huang, K. T., Gaunt, R. F., & Park, Y.-L. (2018). A soft-inflatable exosuit for knee rehabilitation: Assisting swing phase during walking. Frontiers in Robotics and AI, 5, 44. https://doi.org/10.3389/frobt.2018. 00044

[20] Verma, A., & Tiwari, S. (2023). Prevalence of symptomatic knee osteoarthritis and treatment patterns among the rural elderly in northern India. International Journal of Rheumatic Diseases, 26(2), 150–158. https://doi.org/10.1111/ 1756-185X.14470

[21] Wang, D., Wu, Y., Bogue, S. A., & Zhang, X. (2011). An adaptive knee-joint exoskeleton based on biological geometries. In Proceedings of the 2011 IEEE International Conference on Robotics and Automation (pp. 1268–1278). IEEE. https: //doi.org/10.1109/ICRA.2011.5979914

[22] World Bank. (2025). Current health expenditure per capita (current US$) [Data set]. World Development Indicators. https://data.worldbank.org/indicator/SH.XPD.CHEX.PC.CD

[23] World Health Organization. (2022). Global report on assistive technology. World Health Organization. https://www. who.int/publications/i/item/9789240049451

[24] Yalçin, M., Celebi, B., & Patoglu, V. (2013). AssistOn-Knee: A self-aligning knee exoskeleton. In 2013 IEEE/RSJ International Conference on Intelligent Robots and Systems (pp. 987–994). IEEE. https://doi.org/10.1109/IROS. 2013.6696498

[25] Zhang, Y., Ajoudani, A., & Tsagarakis, N. G. (2021). Exo-Muscle: A semi-rigid assistive device for the knee. IEEE Robotics and Automation Letters, 6(4), 8514–8521. https://doi.org/10.1109/LRA.2021.3100609

[26] Cao, J., et al. (2024). A rigid–flexible coupled knee-ankle exoskeleton with Bowden cable actuation. Chinese Academy of Sciences Technical Report.